

Linking endogenous and exogenous popularity processes in social media

Marian-Andrei RIZOIU¹ Lexing XIE¹ Scott SANNER²
Manuel CEBRIAN³ Honglin YU¹ Pascal VAN HENTENRYCK⁴

Abstract

Explaining and predicting the popularity of online multimedia content is an important problem for the practice of information dissemination and consumption. Recent work advances our understanding of popularity, but one important gap remains: to precisely quantify the relationship between the popularity of an online item and the external promotions it receives. This work supplies the missing link between exogenous inputs from public social media platforms (Twitter) and endogenous responses within video content platforms (Youtube). This is done via a novel mathematical model, the Hawkes intensity process, which is able to explain the complex popularity history of each video according to its content, network, and sensitivity to promotion. This model supplies a prototypical description of videos, called an endo-exo map, which allows us to explain the popularity as the joint effects of two intrinsic measures and the amount of discussions from the outside world. This model also allows us to forecast the effects of future promotions more accurately than approaches based on popularity history alone, and to identify videos that have a high potential to become viral, or those for which promotions will have hardly any effect.

Popularity for an online cultural item is the total amount of attention it receives. As an important quantity for measuring collective behavior, popularity is critical for understanding online dissemination for content producers and managing information overload for content consumers. Understanding and predicting popularity has been a topic of recent interest for both researchers and practitioners, but a number of fundamental questions still remain open, such as: What describes the most viral digital items? What roles do intrinsic virality and external promotion play in determining popularity? Can we promote an item to increase its popularity, and how much promotion is needed?

Two main lines of thought shape our current understanding of online popularity. The first corresponds to Crane and Sornette’s [3] view of popularity evolution as a power-law curve as a result of either exogenous shock or endogenous relaxation. The second corresponds to the view that future popularity is best modeled [5] or predicted by past popularity [14] and features regarding the content, author, timing and network context of an online cascade [1, 11]. The points of departure for our work are in two recent observations that suggest more complex models are necessary to understand popularity. We tracked the popularity history of hundreds of thousands of online videos over several years [15], and found that more than 80% do not follow the prototypical power-law dynamic, but have multiple rising or falling phases in different shapes and scales as shown in the videos in Figures 2 and 4. We also observe that volumes of external promotions, such as the sharing of, and tweeting about, a video, are indicative of sudden popularity changes that are otherwise hard to explain as shown in Figures 2(b) and 4(a). More generally, both feature-driven predictions [1, 10, 11, 13, 14] and stochastic event models [16] face fundamental difficulties in independently explaining the complex evolutions of popularity in the presence of external promotions.

In this work, we view popularity dynamics as the continuous interplay between endogenous and exogenous factors. This leads to a novel mathematical model that fills in the missing link between external promotions and internal responses. This model explicitly captures several key factors for each video – the sensitivity to external promotion, content virality, and the temporal decay of network response – which are all estimated from data. Furthermore, we explain the popularity history using aggregated counts rather than individual viewing events, which are unobservable due to privacy and data volume concerns.

¹ The Australian National University and Data61, Canberra, Australia

² University of Toronto

³ Data61, Melbourne, Australia

⁴ University of Michigan

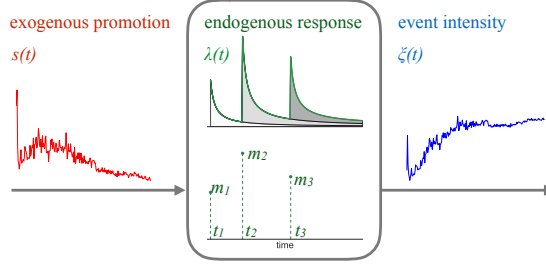


Figure 1: Modeling popularity using a Hawkes intensity process. The input are exogenous sources of promotion or discussions $s(t)$ (in red), that engender endogenous reactions from online social networks (middle box, in green). The endogenous reactions are self-exciting point processes, whose event rate $\lambda(t)$ is a sum of memory kernels triggered by each prior event. In this example, there are three events at time t_1 , t_2 , and t_3 , with respective magnitudes m_1 , m_2 and m_3 (bottom axis). Their contributions to the event rate are shown as white and gray slices, under the curves. The immediate impact of exogenous promotion and the long-term impact due to further endogenous self-excitation combine linearly to form the event intensity $\xi(t)$ over time (in blue).

We design a model specifically for viewcounts by computing expectations over a stochastic event history, and dub it the Hawkes Intensity Process. Figure 11 illustrates the conceptual schema of this model. On the left is the volume of exogenous excitations over time, in the middle is an endogenous self-exciting process that reacts to external input; the output on the right is the popularity series, modeled as the ongoing interaction between the exogenous and endogenous processes. The popularity series modeled through the Hawkes intensity process matches closely with the observed viewcount series, even for videos with complex popularity lifecycles, such as the ones shown in Figure 2.

We present a novel prototype description of each video based on the Hawkes intensity model. This description consists of two quantities – the endogenous response and exogenous sensitivity – readily computed from the history of each video. We use these two quantities to visualize collections of videos on a two-dimensional map, dubbed the *endo-exo map*. Applying the endo-exo map, one can identify videos that have high viral potential, i.e., those with high sensitivity to external promotions and high endogenous response, but not yet popular (e.g., as shown in Figure 4(a)). We can also identify videos for which promotion is unlikely to have an effect, such as those scoring very low in either the endo- or exo-dimension (e.g., as shown in Figure 3(b)).

Another important use of the Hawkes intensity model is to quantify and forecast the effect of future promotions. We validate the forecasting on a collection of 13K+ YouTube videos that are most actively tweeted over a six-month period, and found that forecasts made with the Hawkes intensity model lower the average error made by state-of-the-art history-driven methods by 2 percentile points in overall popularity.

1 The Model

We introduce a model for the evolution of online attention under external influence. First, we use a stochastic point process to link the ongoing effect of external stimuli to the word-of-mouth spread of attention. Next, we propose the Hawkes intensity process, which is a video-specific model for explaining the observed popularity history when the underlying point process is unobserved.

1.1 A point process for endogenous self-excitation

We model the online attention as an exogenously-driven self-exciting process – each viewing *event* is triggered either by a previous event or as a result of external influence. We assume that viewing events of a YouTube video follow a Hawkes point process [7], a type of non-homogenous Poisson point process. In particular, the event rate $\lambda(t)$, a measure of how likely a viewing event will occur in a infinitesimal interval around time t , is determined by two additive components. The first component is proportional to a measure of external influence $s(t)$ scaled by a constant μ . Here $s(t)$ represents the volume of external discussion or promotion over time; it is non-random and is often observed from history, or known from intended promotion plans. The scaling factor μ can be estimated from data for each video. The second component represents the rate of views triggered by a previous event i , which occurred at time t_i with

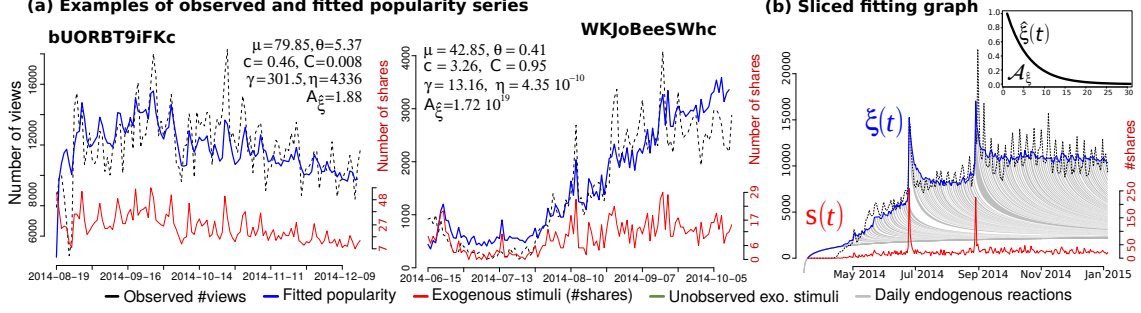


Figure 2: Explaining popularity dynamics using the Hawkes intensity model. (a) Observed popularity history (black dashed), number of shares (red) and popularity as explained by the Hawkes intensity model (blue) on two examples videos: a music video *bUORBT9iFKc* and a News & Politics video *WKJoBeeSWhc*. The complex and multi-phased popularity history cannot be explained by current models such as [3]. (b) A *sliced* fitting graph of a music video (Youtube ID *0bR4LOY94AQ*) – using the impulse response $\xi(t)$ and exogenous stimuli $s(t)$ to explain observed popularity. Each alternating gray and white area is a *slice* of endogenous reaction generated by the external influence in a given day. The total event intensity (blue solid line) is a sum of temporally shifted and scaled versions of $\xi(t)$, which tracks the long-term trends in observed popularity well (dashed line). (inset) Example of the impulse response $\xi(t)$ to one unit of external excitation. The area under this function, A_{ξ} , quantifies the endogenous reaction of a video – it is the total number of views after each unit of exogenous excitation.

magnitude $m_i > 0$, according to a time-decaying triggering kernel $\phi_{m_i}(t - t_i)$. Furthermore, each event $t_i < t$ adds to $\lambda(t)$ independently. This leads to a point process described in Eq. 1.

$$\lambda(t) = \mu s(t) + \sum_{t_i < t} \phi_{m_i}(t - t_i) \quad (1)$$

$$\phi_m(\tau) = \kappa m^{\beta} (\tau + c)^{-(1+\theta)}, \tau \in \mathcal{R}^+ \quad (2)$$

Eq. 2 describes the triggering kernel $\phi(\tau)$. It is designed to capture several key quantities influencing popularity. Parameter κ is a scaling factor for video *quality*. m describes the relative *influence* of the user who generated the event (i.e., m_i in Eq. 1 when multiple events are concerned). β accounts for the nonlinearity between user influence and the effects on popularity. Time interval $\tau = t - t_i$ is the elapsed time since the parent event at t_i ; $c > 0$ is a cutoff term to keep $\phi_m(\tau)$ bounded when τ is small; $1 + \theta$ (for $\theta > 0$) is the power-law exponent for the social system – the larger θ is, the sooner the reaction to an event will stop.

The description above captures the interaction between additive external factors and the endogenous self-exciting effects with a decaying collective memory – such effects are also accumulated over time. This model is an instance of a marked Hawkes process [7] with power-law kernels often found in geophysics [8] and finance [4]. An illustration of this self-exciting process is in Figure 11 – here the overall event rate $\lambda(t)$ (middle) is shown to be a sum of individual memory kernels triggered by events at time t_1, t_2, t_3 with magnitudes m_1, m_2, m_3 , respectively. Moreover, through this self-exciting process, an input time series $s(t)$ engenders the observed popularity series $\xi(t)$, or the aggregate effect of such self-exciting processes, described hereafter.

1.2 The Hawkes intensity process

The point-process description of attention is well-founded, however it has limited applicability since the assumptions about the underlying data are often unrealistic. In particular, due to constraints in user privacy and data volume, what we often observe is the volume of total attention over time rather than the times and properties of individual actions.

To account for this, we introduce the Hawkes intensity $\xi(t)$, the expectation of the event rate $\lambda(t)$ over event history \mathcal{H}_t , consisting of the set of (random) event times and magnitudes up to time t . Such an expected event rate allows us to explain observed event volume over time, without needing to observe individual event times and magnitudes. We found that the intensity $\xi(t)$ is related to the key quantities of the point process analytically (see SI. Sec. 1Details of the Hawkes Intensity Model), and it evolves as

follows:

$$\xi(t) := \mathbb{E}_{\mathcal{H}_t} [\lambda(t)] = \mu s(t) + C \int_0^t \xi(t - \tau) (\tau + c)^{-(1+\theta)} d\tau . \quad (3)$$

Here, event intensity $\xi(t)$ follows a self-consistent integral equation. That is to say, the event intensity at time t is determined by external stimulus $s(t)$, as well as event intensity at a previous time $\xi(t - \tau)$ scaled by its corresponding decay kernel $(\tau + c)^{-(1+\theta)}$ for all temporal offsets $\tau < t$. Note that μ , θ and c were defined in Eq 2, and that κ and β are combined into a positive constant $C = \frac{\kappa(\alpha-1)}{\alpha-\beta-1}$. Here $\alpha > 0$ is the power-law exponent of user influence distribution. Note that the two power law exponents α and θ are distinct in meaning and function, θ defines memory decay over time, while α is determined by the user distribution at large. α is estimated from a large Twitter sample using standard fitting procedures (SI 1.1 The event rate of a marked Hawkes process, [2]). θ and other video-dependent parameters are estimated from popularity history.

The Hawkes intensity model has two novel features for describing popularity. First, it captures the ongoing interactions of exogenous and endogenous effects, and hence able to explain complex popularity series with multiple rises and falls (as shown in Figure 2). State-of-the-art methods lack the capacity of describing such evolutions: Helmstetter and Sornette [8] fit the observed event rate after an initial shock, and Crane and Sornette [3] produce a curve fit on the long-term approximation of the endogenous decay with no exogenous input. Second, this is a generative model for the event intensity series rather than each event, compared to existing settings used in statistics [12] or social networks [16]. In the case of the YouTube data in this article, being able to model popularity series without observing individual viewing events is important for reasons of both data availability (aggregated volume has much less risk for leaking user information) and computation (much more efficient).

1.3 Explaining popularity histories

We estimate model parameters $\{\mu, \theta, C, c\}$ from a history of the number of tweets/shares and views for each video, using non-linear optimization to obtain a least-squares fit (see SI. Sec. 2 Fitting the Hawkes intensity model). Three example fits are shown in Figure 2. Visibly, the event intensity model in Eq 3 links the exogenous and endogenous effects of the social system, resulting in a tight fit between the model and the observed popularity history. For video *bUORBT9iFKc* the memory kernel decays fast ($\theta = 5.37$), and the resulting intensity series tracks the temporal dynamics of the stimuli closely. For video *WKJoBeeSWhc*, the memory kernel decays slowly ($\theta = 0.41$), hence the delayed accumulation of exogenous promotion via the memory kernel results in an overall rising trend.

We can see that only by capturing the non-obvious joint effects from within and outside a social network can a model produce both fine-grained short-term dynamics and accurate long-term trends.

2 Measuring inherent video virality

The Hawkes intensity model describes the inherent properties of a video, in particular its potential to become viral. In this section, we will first introduce two key metrics, the endogenous response and exogenous sensitivity, to quantify different aspects of potential virality of a video. We will then visualize videos on this two-dimensional endo-exo map. This allows us to explain how videos become popular, and look comparatively at videos' popularity and potential with respect to each other. One may think parameters such as scaling factor C and memory exponent θ are good candidates for describing virality. We find, however, that despite being related, the non-linear interactions among the parameters make explaining popularity indirect compared to using the endogenous response described below. Statistics about important model parameters are included in SI Sec. 4 Understanding popularity dynamics.

2.1 Quantifying endogenous response

As shown in the Hawkes intensity model in Eq 3, the total attention a video receives consists of two parts: input from exogenous stimuli, and endogenous response corresponding to non-linear effects accumulated through the integral equation. The first part, sensitivity to external stimuli, is readily quantifiable with scaling parameter μ . We now examine a key property of the model and derive a quantity representing the magnitude of endogenous response.

We observe that the Hawkes intensity model in Eq 3 is a linear time-invariant (LTI) system for $t > 0$. That is to say that if $\xi(t)$ is the event intensity function for input $s(t)$, then (from the same video) the event intensity function for a shifted and scaled version of the input $as(t - t_0)$ is $a\xi(t - t_0)$ for $a > 0, t_0 \geq 0$, i.e., scaled and shifted by the same amount. We show this to be true in SI Sec 1.4 The Hawkes Intensity Process as an LTI system. One important descriptor of the Hawkes intensity process is the event series spawned from one unit of input – called the *impulse response* of a linear system. The complete popularity series is explained as superpositions of such impulse responses over time. Fig 2(c) illustrates this property using a *sliced* and *stacked* popularity graph. In each discrete time point t' , each white or gray *slice* corresponds to a version of the impulse response shifted by t' and scaled by the external stimuli $s(t')$. Adding all these responses together recovers the overall intensity $\xi(t)$ as in Eq 3 (blue line), which tracks closely the long-term dynamics of the observed popularity (dashed line).

Specifically, we define $\hat{\xi}(t)$ as the *impulse response* of a video to a unit impulse of exogenous excitation. From Eq 3 and the descriptions above, we can see that $\hat{\xi}(t)$ is the solution to the following self-consistent integral equation.

$$\hat{\xi}(t) = \delta(t) + C \int_0^t \hat{\xi}(t - \tau)(\tau + c)^{-(1+\theta)} d\tau . \quad (4)$$

An example is shown in Figure 2(b). Here $\delta(t)$ is the Dirac delta function, with $\delta(0) = 1, \delta(t > 0) = 0$. For each video, $\hat{\xi}(t)$ describes its intrinsic response over time. We define the integral of this function over time, $A_{\hat{\xi}} = \int_0^\infty \hat{\xi}(t) dt$, as the total attention generated endogenously by a single unit of exogenous excitation. $A_{\hat{\xi}}$, referred to as *endogenous response*, is related to the branching factor (i.e. the number of direct descendant events) of the underlying Hawkes process. $A_{\hat{\xi}}$ is finite when the branching factor $\frac{C}{\theta c^\theta} < 1$ as shown in SI. Sec. 1.3 Branching factor n and endogenous response $A_{\hat{\xi}}$.

2.2 Visualizing inherent virality with the endo-exo map

Intuitively, a video with a large endogenous response $A_{\hat{\xi}}$ and a high exogenous sensitivity μ has high potential to become viral. Specifically, each unit of exogenous excitation will generate $\mu A_{\hat{\xi}}$ events through the Hawkes intensity process. We construct a 2-dimensional map to visualize $A_{\hat{\xi}}$ and μ for videos – called the *endo-exo map* in the rest of this paper. On this map, videos in close proximity have similar potentials to become popular and the differences in their popularity would be due solely to the difference in exogenous attention. Fig 3(a) illustrates this phenomena using four videos on this endo-exo map. Videos v_1 and v_2 are very similar in both $A_{\hat{\xi}}$ and μ ; the fact that v_1 has 4.61x more views is explained by it receiving 3.22x more exogenous promotions. On the same map, v_4 received a similar amount of promotion as v_1 and their differences in popularity are explained by v_4 being less endogenously responsive (smaller $A_{\hat{\xi}}$) than v_1 . Moreover, v_3 has a similar endogenous response and sees similar amounts of promotion as v_1 ; their differences in popularity are explained by v_3 being less exogenously sensitive, with a lower μ .

2.3 What describes the most popular videos

One may wonder whether higher popularity can be attributed to higher exogenous sensitivity, higher endogenous response or a combination of both. We examine a collection containing diverse video categories and find that the explanation varies. We generate the endo-exo map on a collection 13,738 Youtube videos, called the ACTIVE set – filtered from all 81M tweeted videos over the second half of 2014 with non-trivial amount of tweets and shares (see Materials and Methods).

Figure 3 (c) and (d) compares the density plot on the endo-exo map for videos in **Gaming** and **Film & Animation**, to that of the top 5% in popularity from these two categories, respectively. Visibly, while most popular videos in **Film & Animation** are described by higher exogenous sensitivity (shifting upwards), the most popular **Gaming** videos have higher endogenous response – their density mass is shifted to the right of the endo-exo map. Other categories such as **Comedy** or **News & Politics** (shown in the SI) present two dense regions, one for higher $A_{\hat{\xi}}$ and one for higher μ .

2.4 Identifying unpromotable videos

The endo-exo map can be used to readily identify an interesting class of videos – ones that are very difficult to promote. Given that the quantity $\mu A_{\hat{\xi}}$ describes the number of views that one unit of external promotion will generate under the joint influence of endo- and exo- factors – a very small $\mu A_{\hat{\xi}}$ (e.g.,

$\mu A_{\xi} < 1e - 3$) is a hallmark of a video being *unpromotable*. Figure 3(b) contains a zoomed-out view of the endo-exo map associated with the category **People & Blogs**. We found 63 videos ($\sim 3.2\%$) in this category to be unpromotable. Overall, 549 ($\sim 3.9\%$) videos in the ACTIVE set are deemed unpromotable. The thumbnail of one example video (a teenager video blog) is shown with the figure. It has $\mu = 2.88 \times 10^{-15}$ and $A_{\xi} = 1$, hence each online promotion is expected to generate 0 views. In contrast, for video v_1 in Figure 3(a), each promotion is expected to generate 598 views.

3 Forecasting popularity growth

Via the endo-exo map, the Hawkes intensity process describes a video’s popularity dynamics in the presence of external promotions; this section explores the predictive power of such a model. We first illustrate the setting for popularity forecasts using two examples, and then present a quantitative evaluation.

3.1 Identifying potentially viral videos

We use the Hawkes intensity model to identify videos that are not already popular but have a high potential to become so. This is similar to the phenomenon of delayed recognition in science [9], and we take a model-driven approach that finds such potentially viral items before it becomes popular, rather than a measurement-driven approach that analyze viral items in history. Video *1PuvXpv0yDM* in Figure 4(a) is such an example. As described in the caption, model estimates on this period deem it to have high endogenous response ($A_{\xi} = 6.94 \times 10^{72}$) and high exogenous sensitivity ($\mu = 119.02$). With an additional 229 shares during days 91 to 120, representing more than 6 times the number of shares during the first 90 days, this video drastically improved its ranking in the popularity percentile from 5.85% to 94.9%. This corresponds to having gained 2.42 million views after 120 days.

3.2 Evaluating forecast with historical data

We design a protocol to quantitatively evaluate the predictive power of the Hawkes intensity model. We use historical data held-out over time, thus avoiding the practical difficulty of generating realistic promotions and responses in a large-scale social network. Figure 4(b) illustrates this setting with an example music video. A vertical line divides the observation period, day 1 to 90, and the evaluation period, day 91 to 120. The viewcount and sharing history in the observation period is used to estimate model parameters and explain observed popularity (in blue). Then the model takes as input the exogenous promotion $s(t)$ and estimates the number of views during the evaluation period (in purple). For this example, the forecast and the actual views are fairly similar. Comparing these quantities for a collection of videos will quantify the goodness of forecasting. Such forecast has broader applications than evaluated here. For example, it can be used to both estimate the effect of intended (promotional) interventions, and compare different schedules (amounts of promotion over time) of exogenous interventions for different videos.

3.3 Results

We evaluate the popularity forecast on the ACTIVE set of 13,000+ videos, and measure the forecast quality by absolute error in popularity percentile (see Materials and Methods). Figure 4(c) summarizes forecasting performance for the Hawkes intensity process and baselines for comparison. The state-of-the-art approach for popularity prediction uses multivariate linear regression (MLR) that takes either the historic viewcount [13, 14] or both the viewcount and the promotions as input. MLR is trained on a large collection of videos and we obtain predictions for each video with cross-validation. We can see that the forecasts made using the Hawkes intensity model have lower average error compared to linear regression with exogenous stimuli ($\#$ shares, $\#$ tweets) or without. The best forecast obtained an average percentile error of 4.96% for our model and 6.94% for the baseline, and the differences are statistically significant (paired t-test $p < 0.001$) as shown in SI. Sec. 5.2 Statistical significance. Within the Hawkes intensity model variants, we found that using the number of shares generates slightly better forecast than the number of tweets, but the differences are not statistically significant at $p = 0.001$. We also observe that the performance gap doubles when forecasting popularity on more difficult videos, see SI. Sec. 5 Popularity forecasting and comparison to baseline.

4 Summary and discussion

This research establishes a novel mathematical model to systematically link the endogenous response to the exogenous stimuli of a social system. The model developed here provides a nuanced view of the continued interactions of endogenous and exogenous effects that generate complex and multi-phased popularity dynamics over time. Moreover, we quantitatively describe a video’s inherent potential for becoming viral in terms of the endogenous and exogenous factors, visualized on the endo-exo map. We forecast future popularity under given promotion, obtaining results superior to a state-of-the-art data-driven prediction approach.

We validate the model on the popularity and promotion history of a large set of YouTube videos. We quantify the endogenous virality and exogenous sensitivity for each video, using it to explain the properties of the most popular videos of different content types, as well as to identify videos that will respond well to promotions and those that will not. Such detailed analysis is possible because the collective attention and promotion data are available from YouTube or inferred from public sources such as Twitter. We envision that the same kind of attention dynamics would hold for other content types, such as newspaper page views, podcasts, or blogs.

There are a number of simplifying assumptions and limitations of the proposed model, which can become fruitful directions of further investigation. First, the Hawkes intensity process captures popularity dynamics that are reflected only in the observed external promotion series, and does not capture other behavioral factors such as (daily or weekly) seasonality. What this model focuses on is the *expected* influence over all users rather than individual influence. Both of these observations suggest extensions that could incorporate seasonality components as well as take into account individual influences. Second, the observations in this paper do not directly address causality. We conducted statistical tests using the well-known Granger Causality [6] on the shares and view series (see SI Sec. 4.3 Causal connection between the views, tweets and shares series), which does not show consistent results that either shares influence views or vice versa. Lastly, media items are influenced by a variety of sources in the open online world and there are many sources of external promotion that are unobserved or difficult to obtain data from. A well-known example is that gaming videos are known to be discussed intensively in topic-specific forums. Tracking and estimating diverse or even unknown sources of exogenous influence is another open question for this research area.

5 Materials

5.1 The tweeted videos dataset

We collect a dataset of *tweeted videos* between 2014-05-29 and 2014-12-26 using the Twitter API, which yields a large and diverse sample of over 81 million videos. After restricting to videos that are still online, that have their popularity and sharing history available, and that received at least 100 tweets and 100 shares, and removing 6 rare categories containing less than 1% videos, we are left with a subset of 13,738 videos across 14 categories. A profile of the dataset and details about its construction is given in the SI.

5.2 Popularity percentile and measuring forecasting performance

We construct a popularity percentile scale over a 16 million subset of the 81 million videos whose viewcount history are publicly available (See SI Sec 3.2 The popularity scale over time for details). We map the predicted total viewcount to this percentile scale, and compute the error in the predicted percentile. The percentile-error metric produces meaningful measures across a spectrum of most popular to least popular videos. Compared to error metrics based on the absolute or relative difference in views, this metric focuses on error in the ranking with respect to a large collection of videos. It avoids the error from being skewed by the long-tailed distribution of popularity [1] and focuses on evaluating ranking performance – a measure of practical importance in recommending content or managing a portfolio of media items.

References

- [1] Cheng, J., Adamic, L., Dow, P.A., Kleinberg, J.M., Leskovec, J.: Can cascades be predicted? In: Proceedings of the 23rd International Conference on World Wide Web. pp. 925–936. ACM (2014)

- [2] Clauset, A., Shalizi, C.R., Newman, M.E.J.: Power-Law Distributions in Empirical Data. *SIAM Review* 51(4), 661–703 (Nov 2009), <http://epubs.siam.org/doi/abs/10.1137/070710111>
- [3] Crane, R., Sornette, D.: Robust dynamic classes revealed by measuring the response function of a social system. *Proceedings of the National Academy of Sciences* 105(41), 15649–15653 (2008), <http://www.pnas.org/content/105/41/15649.abstract>
- [4] Embrechts, P., Liniger, T., Lin, L., et al.: Multivariate hawkes processes: an application to financial data. *Journal of Applied Probability* 48, 367–378 (2011)
- [5] Gleeson, J.P., Cellai, D., Onnela, J.P., Porter, M.A., Reed-Tsochas, F.: A simple generative model of collective online behavior. *Proceedings of the National Academy of Sciences* 111(29), 10411–10415 (2014)
- [6] Granger, C.W.: Some recent development in a concept of causality. *Journal of Econometrics* 39(1), 199–211 (1988)
- [7] Hawkes, A.G.: Spectra of some self-exciting and mutually exciting point processes. *Biometrika* 58(1), 83–90 (Apr 1971), <http://biomet.oxfordjournals.org.virtual.anu.edu.au/content/58/1/83.abstract>
- [8] Helmstetter, A., Sornette, D.: Subcritical and supercritical regimes in epidemic models of earthquake aftershocks. *Journal of Geophysical Research: Solid Earth* 107(B10), ESE 10–1–ESE 10–21 (2002)
- [9] Ke, Q., Ferrara, E., Radicchi, F., Flammini, A.: Defining and identifying sleeping beauties in science. *Proceedings of the National Academy of Sciences* 112(24), 7426–7431 (2015)
- [10] Martin, T., Hofman, J.M., Sharma, A., Anderson, A., Watts, D.J.: Exploring limits to prediction in complex social systems. In: *Proceedings of the 25th International Conference on World Wide Web*. pp. 683–694 (2016)
- [11] Milkman, K.L., Berger, J.: The science of sharing and the sharing of science. *Proceedings of the National Academy of Sciences* 111(Supplement 4), 13642–13649 (2014)
- [12] Mohler, G.O., Short, M.B., Brantingham, P.J., Schoenberg, F.P., Tita, G.E.: Self-Exciting Point Process Modeling of Crime. *Journal of the American Statistical Association* 106(493), 100–108 (Mar 2011), <http://www.tandfonline.com/doi/abs/10.1198/jasa.2011.ap09546>
- [13] Pinto, H., Almeida, J.M., Gonçalves, M.A.: Using early view patterns to predict the popularity of youtube videos. In: *Proceedings of the sixth ACM International Conference on Web Search and Data Mining*. pp. 365–374. ACM (2013)
- [14] Szabo, G., Huberman, B.A.: Predicting the popularity of online content. *Communications of the ACM* 53(8), 80–88 (2010)
- [15] Yu, H., Xie, L., Sanner, S.: The lifecycle of a youtube video: Phases, content and popularity. In: *Ninth International AAAI Conference on Web and Social Media* (2015)
- [16] Zhao, Q., Erdogdu, M.A., He, H.Y., Rajaraman, A., Leskovec, J.: Seismic: A self-exciting point process model for predicting tweet popularity. In: *Proceedings of the 21th ACM SIGKDD International Conference on Knowledge Discovery and Data Mining*. pp. 1513–1522. ACM (2015)

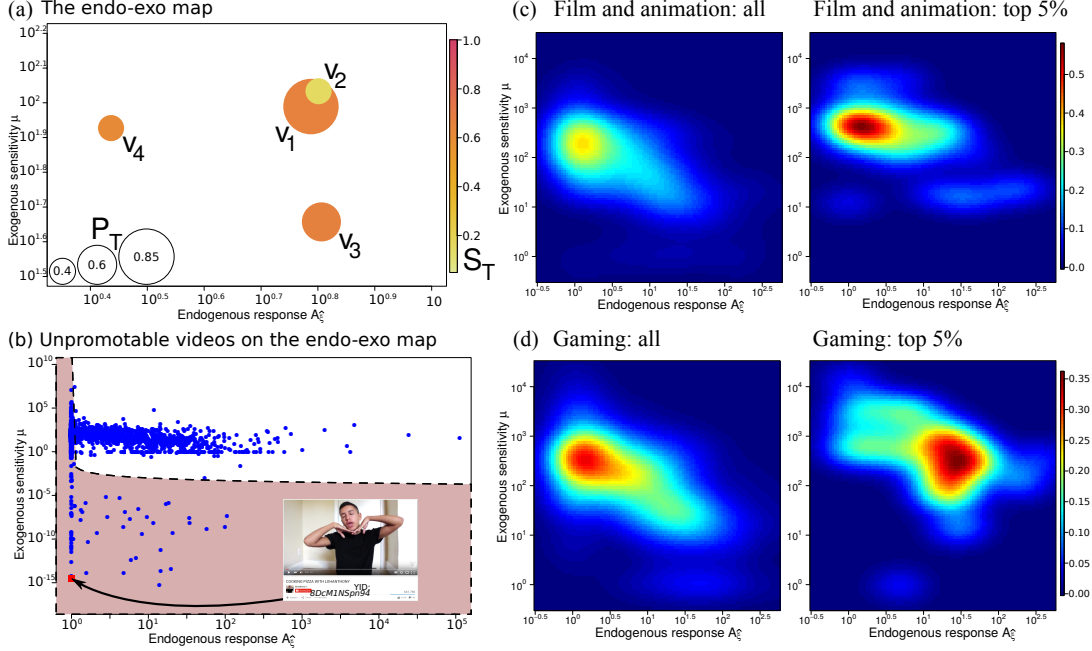


Figure 3: Visualizing video virality and video popularity using the *endo-exo map*. **(a)** Four example videos on the endo-exo map. The x-axis A_ξ represents the magnitude of endogenous reaction. The y-axis represents sensitivity to exogenous stimuli. The radius of each circle is proportional to the *popularity percentile* P_T of each video after $T = 120$ days, with values between 0.0 (least popular) and 1.0 (most popular). The color represents the amount (percentile) of total promotions received, denoted as S_T , with values between 0.0 (no promotion) and 1.0 (receiving the most promotions). v_1 and v_2 present similar endogenous reaction and exogenous sensitivity, being at the same position on the endo-exo map. The difference in their popularity (size) is explained by the fact that v_1 received 3.22 times more promotions than v_2 . Both v_3 and v_4 receive similar amounts of promotion (color) as v_1 , but they achieve lower popularity (smaller size) due to their less privileged position on the endo-exo map: v_3 is less sensitive to external stimuli than v_1 and v_2 , while v_4 has a smaller endogenous reaction than v_1 and v_2 . Information about the four example videos are as follows, with their popularity percentile P_T and promotion percentile S_T (absolute values in parenthesis): v_1 is a short **Gaming** video, YoutubeID *0lTTWeavl1c*, $P_T = 85\%$ (634,370 views), $S_T = 65\%$ (351 shares); v_2 is a collection of “ALS ice bucket challenge” videos, YoutubeID *3hSIhtbiKE*, $P_T = 40\%$ (137,481), $S_T = 10\%$ (109); v_3 is a funny science video, explaining types of infinity in math, YoutubeID *23I5GS4JiDg*, $P_T = 60\%$ (193,052), $S_T = 65\%$ (356); v_4 is from a Portuguese youtuber, YoutubeID *0ndmJzEIcgU*, $P_T = 40\%$ (93,959), $S_T = 60\%$ (311). **(b)** A zoomed-out scatter plot of the endo-exo map of the videos in the **People & Blogs** category. The shaded portion of this map consists of videos with low values of total response $\mu A_\xi < 10^{-3}$ and hence dubbed unpromotable videos. Thumbnail of an example video *8DcM1NSpn94* is included, with $\mu = 2.88 \times 10^{-15}$ and $A_\xi = 1$. **(c)** Density plot for all (left) vs the most popular 5% (right) Film & Animation videos. **(d)** Density plot for all (left) vs the most popular 5% (right) Gaming videos. Popular **Film and Animation** videos tend to have a higher exogenous sensitivity, while those for **Gaming** have mainly a higher endogenous response.

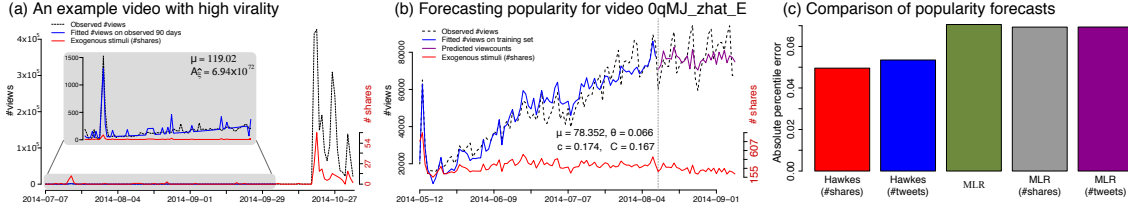


Figure 4: Popularity forecasting using the Hawkes intensity process. (a) Popularity series for video *1PuvXpv0yDM*, explaining a brain disorder. The video receives a total of 36 shares and 15,687 views in the first 90 days (see inset), it is estimated to have a high exogenous sensitivity and a high endogenous response ($\mu = 119.02$, $A_{\xi} = 6.94 \times 10^{72}$). Between day 91 and day 120, this video *jumped* from a popularity percentile of 5.85% to 94.9%, receiving 229 shares and gaining 2.42 million views. (b) Forecasting popularity for video *0qMJ_zhat_E*. Black dotted line: viewcounts series from day 1 to 120 after video upload. Red line: exogenous stimuli $s(t)$, also used in parameters estimation. Left of the gray dashed vertical line at $T \leq 90$ days: time period used for parameters estimation. Blue line: fitted viewcounts for $T \leq 90$ days, generated using Eq 3. Magenta line: viewcount forecast for day 91 to 120. (c) Comparison of average forecasting errors on the ACTIVE set. y-axis: Forecasting errors, calculated as the absolute difference between the popularity percentile at day 120 and that forecasted by each approach. x-axis, left to right: Hawkes intensity model, using either #shares or #tweets as $s(t)$; multivariate linear regression (MLR), using only popularity history, or #shares and #tweets, respectively.

Supporting Information

“Linking endogenous and exogenous popularity processes in social media”

Marian-Andrei Rizoio, Lexing Xie, Scott Sanner, Manuel Cebrian, Honglin Yu, and Pascal Van Hentenryck

Contents

1	Details of the Hawkes Intensity Model	1
1.1	The event rate of a marked Hawkes process . . .	1
1.2	Deriving the expected event rate $\xi(t)$ for unobserved point processes	1
	Preliminaries: Event rate and the counting process	1
	Expected event rate for <i>unmarked</i> Hawkes processes	2
	Expected event rate for <i>marked</i> Hawkes processes	3
1.3	Branching factor n and endogenous response A_ξ	4
1.4	The Hawkes Intensity Process as an LTI system	4
2	Fitting the Hawkes intensity model	5
2.1	Settings for model estimation	5
2.2	Computing gradients	5
2.3	Adding an \mathcal{L}^2 regularizer	6
3	Data	6
3.1	The 5Mo and ACTIVE datasets	6
3.2	The popularity scale over time	7
4	Understanding popularity dynamics	8
4.1	Behavior across groups of videos: categories and channels	8
4.2	What makes videos popular	11
4.3	Causal connection between the views, tweets and shares series	12
5	Popularity forecasting and comparison to baseline	13
5.1	Additional results	13
5.2	Statistical significance	13
	Statistical testing with large sample size	13
	Experimental setup	13
	No performance difference between the two exogenous stimuli sources	14
	Significant difference between the Hawkes model and MLR	14
5.3	Forecasting performance on difficult videos . .	14

1 Details of the Hawkes Intensity Model

Given time $t \in [0, \infty)$, we denote by $\lambda(t)$ the *event rate* of an online resource at time t . The goal of this section is to derive the *expected event rate*, denoted as $\xi(t)$, as the average response rate from a large network.

There are two sources of events in the social system – *exogenous* events originating outside the system and *endogenous* events spawned from within the system as the response to previous events (that are either exogenous or endogenous). For example, a public speech held by a famous politician can be an exogenous source for the number of views of relevant Youtube videos on politics; on the other hand, the views on trailers prior to the release of new movies exhibits a rich-get-richer effect for attention distribution that are characteristic of endogenous word-of-mouth diffusion.

1.1 The event rate of a marked Hawkes process. The Hawkes process [5], as defined in main text Eq. 1, is a non-

homogeneous Poisson process with self-excitation, its event rate $\lambda(t)$, or instantaneous conditional intensity $r(t|\mathcal{H}_t)$ is:

$$\lambda(t) := r(t|\mathcal{H}_t) = \mu s(t) + \sum_{t_i < t} \phi_{m_i}(t - t_i) \quad [1]$$

Here $t > 0$ denotes time; $\mathcal{H}_t = \{(m_i, t_i); t_i < t\}$ is the event history before time t ; $s(t)$ is the rate of exogenous events. μ is a scaling factor for exogenous stimulus, and $\phi_m(\tau)$ is a time-decaying trigger kernel that is determined by the magnitude of each event m_i .

Our Hawkes intensity model is a type of *marked Hawkes process*, as also used in [6, 11]. In marked Hawkes processes, each event i has an occurrence time t_i and a magnitude m_i (or mark), which captures the relative amplification of the likelihood of an event to spawn future events. Intuitively, the mark can represent the magnitude of an earthquake when modeling the occurrence of aftershocks of an earthquake, or the number of people an event can subsequently influence when modeling social networks. This can be approximated, say, with the number of followers or friends. The triggering kernel $\phi_m(\tau)$, as defined in main text Eq. 2, can be written as the product of two separable terms: $b(m)$ modeling the influence of event marks and $\phi(\tau)$ modeling the temporal decay:

$$\begin{aligned} \phi_m(\tau) &= \kappa m^\beta \hat{\tau}^{-(1+\theta)} := b(m)\phi(\tau), \\ \text{with } b(m) &= \kappa m^\beta, \phi(\tau) = \hat{\tau}^{-(1+\theta)}, \hat{\tau} = \tau + c. \end{aligned} \quad [2]$$

Note $\hat{\tau} = \tau + c$ introduced for the sake of brevity in the calculations in the following sections.

In this work, we focus on modeling the total attention – commonly known as popularity, that closely connects to the average event rate across the whole network. We extract the number of followers m for a large sample of users from our dataset described in Sec. 3 and fit a power-law distribution $p(m) = (\alpha - 1)m^{-\alpha}$ following the method in [1]. We obtain $\alpha = 2.016$ and we use it throughout the experiments. As noted in the main text, the two power law exponents are distinct in meaning and function, θ defines memory decay over time, while α is determined by the user distribution at large. α is estimated from a large Twitter sample. θ and other video-dependent parameters are estimated from popularity history as detailed in Sec 2 below.

1.2 Deriving the expected event rate $\xi(t)$ for unobserved point processes. The goal of this section is to derive the *expected event rate* $\xi(t)$ over time as specified in the main text Eq 3. This is done in three steps: we first include a preliminary description of the event rate $\lambda(t)$ in terms of the underlying counting process over infinitesimal intervals, we then derive the expected event rate for *unmarked* Hawkes processes, and finally we build upon these to derive the expected event rate for *marked* Hawkes processes.

Preliminaries: Event rate and the counting process

It is well known in stochastic process literature [8] that the event rate $\lambda(t)$, or the *conditional intensity specification* $r(t|\mathcal{H}_t)$ of a point process is completely characterized by the corresponding counting process $N(t)$. Here $N(t)$ is the total number of events observed between time 0 and t .

Given an infinitesimal interval δ at time t , the relationship between $N(t)$ and $r(t|\mathcal{H}_t)$ is described as:

$$\begin{aligned} \mathbb{P}(N(t+\delta) - N(t) = 1|\mathcal{H}_t) &= r(t|\mathcal{H}_t)\delta + o(\delta) , \\ \mathbb{P}(N(t+\delta) - N(t) > 1|\mathcal{H}_t) &= o(\delta) , \\ \text{with } \lim_{\delta \downarrow 0} \frac{o(\delta)}{\delta} &= 0 . \end{aligned} \quad [3]$$

Here \mathbb{P} denotes the probability of a discrete random variable. The intuition of the expression above is that $r(t|\mathcal{H}_t)$ is proportional to the probability that $N(t)$ increments by 1, and that it is “very unlikely” for $N(t)$ to increment by more than one.

Let dN_t be the counting increment $N(t+\delta) - N(t)$ as $\delta \downarrow 0$. From Eq 3, we can describe dN_t as a Bernoulli random variable, with:

$$\begin{aligned} \mathbb{P}(dN_t = 1|\mathcal{H}_t) &= r(t|\mathcal{H}_t)\delta , \\ \mathbb{P}(dN_t = 0|\mathcal{H}_t) &= 1 - r(t|\mathcal{H}_t)\delta , \\ \text{for } \delta \downarrow 0 . \end{aligned}$$

It follows from the above that

$$E_{dN_t|\mathcal{H}_t}[dN_t] = r(t|\mathcal{H}_t)\delta, \text{ for } \delta \downarrow 0.$$

Using the shorthand $\lambda(t)$ for event rate and putting the above together, we can see that Hawkes processes can be specified as:

$$\begin{aligned} \lambda(t) &:= r(t|\mathcal{H}_t) = \lim_{\delta \downarrow 0} \frac{\mathbb{P}(N(t+\delta) - N(t) = 1|\mathcal{H}_t)}{\delta} \\ &= \lim_{\delta \downarrow 0} \frac{\mathbb{P}(dN_t = 1|\mathcal{H}_t)}{\delta} \\ &= \lim_{\delta \downarrow 0} \frac{E_{dN_t|\mathcal{H}_t}[dN_t]}{\delta} , \end{aligned} \quad [4]$$

Note that Eq. 4 is an alternate formulation of Eq. 1 through the counting process $N(t)$. Eq. 4 holds for all non-homogeneous Poisson processes. Hawkes processes (marked and unmarked) are special cases of non-homogeneous Poisson processes.

Expected event rate for *unmarked* Hawkes processes

We first study the simpler case of an *unmarked* Hawkes processes $\lambda^u(t)$, and derive its expected event rate $\xi^u(t)$ over possible event histories. While it is not strictly necessary to breakdown the derivation into two parts, this helps illustrate the main ideas underlying the derivation for *marked* processes in the next subsection. The key idea in this subsection is converting the conditional expectation of event history into increments of the counting process, and using conditional expectations to link the expectations of counting increments to the expected rate $\xi^u(t)$ via $\lambda^u(t)$. The next subsection will use exactly the same treatment for the history of event times, and performs a similar treatment for a history of event magnitudes.

Let an unmarked Hawkes process be:

$$\lambda^u(t) := r(t|\mathcal{H}_t) = \mu s(t) + \sum_{t_i < t} \phi(t - t_i). \quad [5]$$

Here $\phi(\tau)$ is a memory kernel specified in Eq 2, scaling constant κ is omitted without loss of generality. Note Eq. 4 still holds. Here $i = 1, \dots, N(t)$ is the event index, and $N(t)$ is a random variable, representing the total number of events before time t , i.e. the counting process. It is worth noting that there are two equivalent expressions of the event history \mathcal{H}_t .

The first one is \mathcal{H}_t being a *random* set of time stamps of the events which took place between $[0, t]$, $\mathcal{H}_t = \{t_{1:N(t)}\}$. Note that the cardinality of \mathcal{H}_t is $N(t)$, hence random. The second definition expresses \mathcal{H}_t with the counting process $N(\tau)$ as a piece-wise constant function between $[0, t]$. Here each jump point in $N(\tau)$ correspond to an event time, and the number of jumps is random variable $N(t)$. It is easy to see that the two definitions are equivalent. For convenience, we write $\mathcal{H}_t = \{N(\tau), 0 < \tau < t\}$.

We define the expected event rate $\xi^u(t)$ as a function over time, obtained by taking expectations of $\lambda^u(t)$ over the event history, note that this is an *unmarked* process, all event magnitudes are the same (i.e. 1). Note that taking expectations over \mathcal{H}_t can be thought of as either over a set of random variables t_i with a random dimensionality $N(t)$, or as over random piece-wise constant functions over time, i.e. $N(\tau)$, for $0 < \tau < t$.

$$\begin{aligned} \xi^u(t) &:= \mathbb{E}_{\mathcal{H}_t}[\lambda^u(t)] \\ &= \mathbb{E}_{\mathcal{H}_t} \left[\mu s(t) + \sum_{t_i < t} \phi(t - t_i) \right] \\ 6(a) &= \mu s(t) + \mathbb{E}_{t_{1:N(t)}} \left[\sum_{i=1}^{N(t)} \phi(t - t_i) \right] \\ 6(b) &= \mu s(t) + \mathbb{E}_{\{N(\tau), 0 < \tau < t\}} \left[\lim_{\delta \downarrow 0} \sum_{k=1}^K \mathbf{1}(dN_{k\delta} = 1) \phi(t - k\delta) \right] \\ 6(c) &= \mu s(t) + \lim_{\delta \downarrow 0} \mathbb{E}_{dN_{k\delta}, k=1:K} \left[\sum_{k=1}^K \mathbf{1}(dN_{k\delta} = 1) \phi(t - k\delta) \right] \end{aligned} \quad [6]$$

Here step 6(a) is due to $\mu s(t)$ being not random, and that expectations over all $t_{1:N(t)}$ are equivalent to taking expectations over event history \mathcal{H}_t .

In step 6(b), we divide time interval $(0, t)$ into K equal-sized infinitesimal intervals of size *delta*, with $K\delta = t$. $\mathbf{1}(dN_{k\delta} = 1)$ is the indicator function that takes value 1 when there is an event in the interval $[(k-1)\delta, k\delta)$, or $dN_{k\delta} = 1$, and 0 otherwise. Note that we replaced each arrival time t_i from line 6(a) with $k\delta$, since event i occurred in the time interval $[(k-1)\delta, k\delta)$. Consequently, the term $\phi(t - t_i)$ became $\phi(t - k\delta)$.

In step 6(c), we first exchange the order of the limit $\lim_{\delta \downarrow 0}$ and expectation. We note that taking expectation over the counting process $\{N(\tau), 0 < \tau < t\}$ is equivalent to taking expectation over its Bernoulli increments $\{dN\tau, 0 < \tau < t\}$, or it’s discretized version over infinitesimal intervals $dN_{k\delta}, k=1:K$.

We then unroll the sum over all intervals. For an interval $k'\delta$, or $[(k'-1)\delta, k'\delta)$, the indicator function becomes $\mathbf{1}(dN_{k'\delta} = 1)$, the kernel $\phi(t - k'\delta)$, and the expectation is taken over $dN_{k\delta}, k=1:k'$ since the process is causal – i.e. current events are only influenced by the past and not the future.

$$\begin{aligned} &\mathbb{E}_{dN_{k\delta}, k=1:K} \left[\sum_{k=1}^K \mathbf{1}(dN_{k\delta} = 1) \phi(t - k\delta) \right] \\ &= \mathbb{E}_{dN_{k\delta}, k=1} [\mathbf{1}(dN_{1\delta} = 1) \phi(t - 1\delta)] \\ &\quad + \mathbb{E}_{dN_{k\delta}, k=1,2} [\mathbf{1}(dN_{2\delta} = 1) \phi(t - 2\delta)] \\ &\quad + \dots \\ &\quad + \mathbb{E}_{dN_{k\delta}, k=1:k'} [\mathbf{1}(dN_{k'\delta} = 1) \phi(t - k'\delta)] \\ &\quad + \dots \\ &\quad + \mathbb{E}_{dN_{k\delta}, k=1:K} [\mathbf{1}(dN_{K\delta} = 1) \phi(t - K\delta)] \end{aligned} \quad [7]$$

Each expectation term in Eq. 7 can be computed as follows.

$$\begin{aligned}
 & \mathbb{E}_{dN_{k\delta}, k=1:k'} [\mathbf{1}(dN_{k'\delta} = 1)\phi(t - k'\delta)] \\
 (8a) \quad &= \mathbb{E}_{\mathcal{H}_{(k'-1)\delta}} \mathbb{E}_{dN_{k'\delta} | \mathcal{H}_{(k'-1)\delta}} [\mathbf{1}(dN_{k'\delta} = 1)] \phi(t - k'\delta) \\
 (8b) \quad &= \delta \mathbb{E}_{\mathcal{H}_{(k'-1)\delta}} [\lambda^u(k'\delta)] \phi(t - k'\delta) \\
 (8c) \quad &= \delta \xi^u(k'\delta) \phi(t - k'\delta) ; \quad [8]
 \end{aligned}$$

Step (8a) is due to the kernels term $\phi(t - k'\delta)$ being non-random and thus becoming constants. Also note that each expectation $\mathbb{E}_{dN_{k\delta}, k=1:k'} [\mathbf{1}(dN_{k'\delta} = 1)]$ can be computed by breaking down the joint distribution $dN_{k\delta}, k=1:k'$ into the conditional distribution $dN_{k'\delta} | \mathcal{H}_{(k'-1)\delta}$ and the prior distribution over $\mathcal{H}_{(k'-1)\delta}$. We write the prior in terms of event history for notational convenience. Due to the two equivalent definitions of event history, taking the expectation over the history $\mathcal{H}_{(k'-1)\delta}$ is equivalent to taking the expectation over increments of the counting process $E_{dN_{k\delta}, k=1:(k'-1)}$.

Step (8b) is due to Eq. 4, the inner expectation can be written as $\mathbb{E}_{dN_{k'\delta} | \mathcal{H}_{(k'-1)\delta}} [\mathbf{1}(dN_{k'\delta} = 1)] = \delta \lambda^u(k'\delta)$ as $\delta \downarrow 0$.

Step (8c) is due to the definition of the expected event rate $\xi^u(t)$ in Eq. 6. The expectation of event rate $\lambda^u(k'\delta)$ over $\mathcal{H}_{(k'-1)\delta}$ becomes $\xi^u(k'\delta)$ as $\delta \downarrow 0$.

Applying the result of Eq. 8 back to Eq. 7, we get:

$$\mathbb{E}_{dN_{k\delta}, k=1:K} \left[\sum_{k=1}^K \mathbf{1}(dN_{k\delta} = 1) \phi(t - k\delta) \right] = \sum_{k=1}^K \delta \xi^u(k\delta) \phi(t - k\delta) \quad [9]$$

Applying Eq. 9 to the end of Eq. 6, and taking the limit $\delta \downarrow 0$, we have:

$$\begin{aligned}
 \xi^u(t) &:= \mathbb{E}_{\mathcal{H}_t} [\lambda^u(t)] \\
 t=K\delta \quad &= \mu s(t) + \lim_{\delta \downarrow 0} \sum_{k=1}^K \delta \xi^u(k\delta) \phi(t - k\delta) \\
 &= \mu s(t) + \int_0^t \xi^u(\tau) \phi(t - \tau) d\tau \quad [10]
 \end{aligned}$$

Performing a change of variable $\tau \leftarrow t - \tau$, we obtain the integral equation specifying the expected event rate for unmarked Hawkes process.

$$\xi^u(t) = \mu s(t) + \int_0^t \xi^u(t - \tau) \phi(\tau) d\tau \quad [11]$$

To the best of our knowledge, this definition of the intensity function, along with the derivation of its analytical form is new. The original paper by Hawkes [5] presents an integral equation of similar form, but it is for the covariance density and not the event intensity function.

Expected event rate for *marked* Hawkes processes

The *expected event rate function* $\xi(t)$ for a *marked* Hawkes process is defined as the expectation of the event rate function $\lambda(t)$ over the set of event times and magnitudes before time t . In this subsection we work with the event rate as specified in Eq. 1.

$$\lambda(t) := r(t | \mathcal{H}_t) = \mu s(t) + \sum_{t_i < t} \phi_{m_i}(t - t_i)$$

In this subsection, the definition of even history is augmented with event magnitudes. i.e., $\mathcal{H}_t = \{(t_i, m_i), i=1:N(t)\}$, i.e., each event consists of a (random) jump time t_i and a (random) event magnitude m_i , and there are $N(t)$ (another random quantity) such time-magnitude pairs. We assume that

any event magnitude m_i is drawn *iid* from the same power-law distribution $p(m) = (\alpha - 1)m^{-\alpha}$, $m > 0$, once the event time t_i is determined. That is to say, for an event spawned through the endogenous process, the magnitude of the event is independent of the magnitude of its parent event.

We define the expected event rate $\xi(t)$ for the *marked* Hawkes processes $\lambda(t)$ as follows. Step (12a) below is due to $\mu s(t)$ being non-random.

$$\begin{aligned}
 \xi(t) &:= \mathbb{E}_{\mathcal{H}_t} [\lambda(t)] \\
 &= \mathbb{E}_{\mathcal{H}_t} \left[\mu s(t) + \sum_{t_i < t} \phi_{m_i}(t - t_i) \right] \\
 Eq.2 \quad &= \mathbb{E}_{\mathcal{H}_t} \left[\mu s(t) + \sum_{t_i < t} b(m_i) \phi(t - t_i) \right] \\
 (12a) \quad &= \mu s(t) + \mathbb{E}_{\mathcal{H}_t} \left[\sum_{i=1}^{N(t)} b(m_i) \phi(t - t_i) \right] \quad [12]
 \end{aligned}$$

In order to unroll this expectation into K small intervals of size δ , we need a set of auxiliary variables, called $m_k, k = 1 : K$. For each interval $[(k-1)\delta, k\delta]$, we draw $m_k \sim p(m)$. If indicator function $\mathbf{1}(dN_{k\delta} = 1) = 1$, then m_k is *kept*; otherwise when $\mathbf{1}(dN_{k\delta} = 1) = 0$, m_k is *thrown away* as no event happened in this interval. One can easily verify that this process of *iid* draws of m_k is equivalent to *iid* draws of the original m_i . We use this to re-write the expectation in Eq. 12, and exchange the order of the expectation and the limit.

$$\begin{aligned}
 & \mathbb{E}_{\mathcal{H}_t} \left[\sum_{i=1}^{N(t)} b(m_i) \phi(t - t_i) \right] \\
 &= \mathbb{E}_{\mathcal{H}_t} \left[\lim_{\delta \downarrow 0} \sum_{k=1}^K \mathbf{1}(dN_{k\delta} = 1) b(m_k) \phi(t - k\delta) \right] \\
 &= \lim_{\delta \downarrow 0} \mathbb{E}_{\mathcal{H}_t} \left[\sum_{k=1}^K \mathbf{1}(dN_{k\delta} = 1) b(m_k) \phi(t - k\delta) \right] \quad [13]
 \end{aligned}$$

We exchange the order of the expectation and the summation, and unroll the sum over all intervals. This is similar to Eq. 7. The causal property of marked Hawkes process means that the expectation of each term $[\mathbf{1}(dN_{k\delta} = 1) b(m_k) \phi(t - k\delta)]_{k=k'}$ only depends on event history $\mathcal{H}_{k'\delta}$, and not after.

$$\begin{aligned}
 & \mathbb{E}_{\mathcal{H}_t} \left[\sum_{k=1}^K \mathbf{1}(dN_{k\delta} = 1) b(m_k) \phi(t - k\delta) \right] \\
 &= \mathbb{E}_{\mathcal{H}_{1\delta}} [\mathbf{1}(dN_{1\delta} = 1) b(m_1) \phi(t - \delta)]_{k=1} \\
 & \quad + \mathbb{E}_{\mathcal{H}_{2\delta}} [\mathbf{1}(dN_{2\delta} = 1) b(m_2) \phi(t - 2\delta)]_{k=2} \\
 & \quad + \dots \\
 & \quad + \mathbb{E}_{\mathcal{H}_{k'\delta}} [\mathbf{1}(dN_{k'\delta} = 1) b(m_{k'}) \phi(t - k'\delta)]_{k=k'} \\
 & \quad + \dots \\
 & \quad + \mathbb{E}_{\mathcal{H}_{K\delta}} [\mathbf{1}(dN_{K\delta} = 1) b(m_K) \phi(t - K\delta)]_{k=K} \quad [14]
 \end{aligned}$$

We now compute the expectation term when $k = k'$. Step (15a) is due to $\phi(t - k'\delta)$ being non-random. Step (15b) breaks down the expectation over the entire history $\mathcal{H}_{k'\delta}$ into the part over the current event (and its magnitude if happens) $dN_{k'\delta}, m_{k'}$ conditioned on prior history $\mathcal{H}_{(k'-1)\delta}$ and over the

prior history itself. This is similar to Eq. 8 for the unmarked process.

$$\begin{aligned}
 & \mathbb{E}_{\mathcal{H}_{k'\delta}} [\mathbf{1}(dN_{k\delta} = 1)b(m_k)\phi(t - k\delta)]_{k=k'} \\
 (15a) &= \mathbb{E}_{\mathcal{H}_{k'\delta}} [\mathbf{1}(dN_{k'\delta} = 1)b(m_{k'})]\phi(t - k'\delta) \\
 (15b) &= \mathbb{E}_{\mathcal{H}_{(k'-1)\delta}} \mathbb{E}_{dN_{k'\delta}, m_{k'} | \mathcal{H}_{(k'-1)\delta}} [\mathbf{1}(dN_{k'\delta} = 1)b(m_{k'})]\phi(t - k'\delta)
 \end{aligned} \quad [15]$$

Note that the middle conditional expectation term decomposes into two parts. Note that $\mathbf{1}(dN_{k'\delta} = 1)$ is independent of $m_{k'}$, therefore

$$\mathbb{E}_{dN_{k'\delta} | \mathcal{H}_{(k'-1)\delta}} [\mathbf{1}(dN_{k'\delta} = 1)] = \delta\lambda(k'\delta); \text{ as } \delta \downarrow 0 \quad [16]$$

The expectation of function $b(m)$ is the same and only depends on $p(m)$ whenever $dN_{k'\delta} = 1$. This is due to the generating assumption of event magnitudes at the beginning of this subsection.

$$\mathbb{E}_{dN_{k'\delta}, m_{k'} | \mathcal{H}_{(k'-1)\delta}} [b(m_{k'})] = \mathbb{E}_m [b(m)] \quad [17]$$

Furthermore, we see that $\mathbb{E}_m [b(m)]$ can be computed in closed form, we call this modeling constant C .

$$\begin{aligned}
 \mathbb{E}_m [b(m)] &= \mathbb{E}_m [\kappa m^\beta] = \kappa \int_1^\infty p(m) m^\beta dm \\
 &= \kappa \int_1^\infty (\alpha - 1) m^{-\alpha} m^\beta dm = \frac{\kappa(\alpha - 1)}{\alpha - \beta - 1} := C
 \end{aligned} \quad [18]$$

Plugging in the result of Eq. 16–18 back to Eq.15, we notice $\mathbb{E}_{\mathcal{H}_{(k'-1)\delta}} [\lambda(k'\delta)] = \xi(k'\delta)$ due to the definition of $\xi(t)$ in Eq. 12, which yields

$$\mathbb{E}_{\mathcal{H}_{k'\delta}} [\mathbf{1}(dN_{k\delta} = 1)b(m_k)\phi(t - k\delta)]_{k=k'} = C \cdot \delta\xi(k'\delta). \quad [19]$$

Applying this result to Eq. 14 and then to Eq.12, followed by taking the limit $\delta \downarrow 0$, we have:

$$\begin{aligned}
 \xi(t) &:= \mathbb{E}_{\mathcal{H}_t} [\lambda(t)] \\
 t=K\delta &= \mu s(t) + \lim_{\delta \downarrow 0} \sum_{k=1}^K C \cdot \delta\xi(k\delta)\phi(t - k\delta) \\
 &= \mu s(t) + C \int_0^t \xi(\tau)\phi(t - \tau)d\tau \\
 \tau \leftarrow t - \tau &= \mu s(t) + C \int_0^t \xi(t - \tau)\phi(\tau)d\tau \\
 \phi(\tau) = \hat{\tau}^{-(1+\theta)} &= \mu s(t) + C \int_0^t \xi(t - \tau)\hat{\tau}^{-(1+\theta)}d\tau
 \end{aligned} \quad [20]$$

Eq. 20 is Eq. 3 in the main text.

1.3 Branching factor n and endogenous response A_ξ . We derive two quantities from the Hawkes Intensity Process in order to better visualize and explain the diverse behavior of video popularity.

The first key parameter is the branching factor n , defined as the mean number of daughter events generated by a mother event. For a marked Hawkes point process, the branching factor is computed by integrating the triggering kernel over time and taking the expectation over the magnitude m .

$$\begin{aligned}
 n &= \int_{m_{min}}^\infty \int_0^\infty p(m)\phi_m(\tau)d\tau dm = \\
 &= \frac{C}{\theta c^\theta}, \text{ for } \beta < \alpha - 1 \text{ and } \theta > 0.
 \end{aligned}$$

$n < 1$ implies a *subcritical regime*, i.e., the instantaneous rate of events decreases over time and the number of new events will eventually cease to occur (in probability); $n > 1$ implies a *supercritical regime*, i.e. each new event generates more than one direct descendant, which in turn generates more descendants, unless the network condition changes, the total number of events is expected to be infinity.

The second quantity A_ξ , as defined in the main text *Measuring inherent video virality*, is the total number of (direct and indirect) descendants generated from one event. In the main text it is defined as an integral over the impulse response $A_\xi = \int_0^\infty \hat{\xi}(t)dt$.

Although defined separately, we can see that A_ξ is closely related to branching factor n : the initial exogenous event will generate n events as first-generation direct descendants. Each of these events will generate an expected n events (n^2 events in the second generation), and each of these will in turn generate n events (n^3 events in the third generation), ... Here n^k is the average number of events in the k^{th} generation, and so on. This leads to an equivalent definition of A_ξ .

$$\begin{aligned}
 A_\xi &= 1 + n + n^2 + \dots + n^k + \dots = \\
 &= \lim_{k \rightarrow \infty} \frac{1 - n^k}{1 - n} = \\
 &= \begin{cases} \frac{1}{1-n} & , n < 1 \\ \infty & , n > 1 \end{cases}
 \end{aligned} \quad [21]$$

While both capturing the endogenous property of the Hawkes Intensity model, A_ξ and n emphasize different intuitions. We chose to visualize A_ξ in the endo-exo map, because it has a direct correspondence to the *sliced LTI system* view in main text Eq. 4 and Figure 2, and that A_ξ has better numerical resolution for the more viral videos – i.e., when n is close to 1. In the main text, we obtain estimates of A_ξ by numerically integrating $\hat{\xi}$ in Eq. 4 to $t = 10,000$ discrete time steps.

Crane and Sornette [3] showed that the Hawkes Intensity Process in a super-critical state could explain some rising patterns of popularity observed in social media. We note, however, that finite resources in the real world, such as collective human attention [10], are bound to be exhausted and online systems cannot stay indefinitely in a supercritical regime. We argue, most online media items are affected by a continued interaction of exogenous stimuli and endogenous reaction (that may be sub- or super- critical), leading to continued rise in popularity, or multiple phases of rising and falling patterns.

1.4 The Hawkes Intensity Process as an LTI system. The Hawkes intensity process can be viewed as a system with one input – the exogenous stimuli rate $s(t)$, and one output – the event rate $\xi(t)$. The Main Text claimed that the system $s(t) \rightarrow \xi(t)$ is an Linear Time Invariant (LTI) system. That is to say, the system has two properties:

Linearity, which states that the relation between the input and the output of the system is a linear map: if $s_1(t) \rightarrow \xi_1(t)$ and $s_2(t) \rightarrow \xi_2(t)$, then $as_1(t) + bs_2(t) \rightarrow a\xi_1(t) + b\xi_2(t)$, $\forall a, b \in \mathbb{R}$. We can see that linear scaling is true $as_1(t) \rightarrow a\xi_1(t)$ by multiplying a to both sides of Eq. 3 in the main text and regrouping terms. Additivity $as_1(t) + bs_2(t) \rightarrow a\xi_1(t) + b\xi_2(t)$ can be shown similarly.

Time invariance, which states that the response to a delayed input is identical and similarly delayed: if $s(t) \rightarrow \xi(t)$ then $s(t - t_0) \rightarrow \xi(t - t_0)$.

We wish to show the following for Eq. 3 of the main text:

$$\xi(t - t_0) = \mu s(t - t_0) + C \int_0^t \hat{\tau}^{-(1+\theta)} \xi(t - t_0 - \tau) d\tau$$

After a change of variable $t' = t - t_0$, we can see that the LHS is $\xi(t')$. For the RHS, $\hat{\tau}$ remains unchanged, the rest is:

$$\mu s(t') + C \int_0^{t'+t_0} \hat{\tau}^{-(1+\theta)} \xi(t' - \tau) d\tau$$

We write the integral into two parts, i.e., $(0, t)$ and $(t', t' + t_0)$.

$$\mu s(t') + C \int_0^{t'} \hat{\tau}^{-(1+\theta)} \xi(t' - \tau) d\tau + C \int_{t'}^{t'+t_0} \hat{\tau}^{-(1+\theta)} \xi(t' - \tau) d\tau$$

We note that $\xi()$ is a causal function, i.e., $\xi(t) = 0$ for $t < 0$, or $\xi(t' - \tau) = 0$ for $\tau > t'$. The second term vanishes. RHS becomes

$$\mu s(t') + C \int_0^{t'} \hat{\tau}^{-(1+\theta)} \xi(t' - \tau) d\tau$$

Note LHS = RHS due to Equation 20 and time invariance holds.

The LTI property directly implies the following about Hawkes intensity processes, as illustrated in Figure 2 of the main text.

- *Additive effects from multiple sources of external stimulation:* when applying two sources of excitation, the event rate of the resulting Hawkes intensity process is the sum of the rates generated by each source of excitation independently. This allows us to separately quantify the impact of each source.
- *Scaling the expected event rate:* if the exogenous stimuli scales up or down, the endogenous reaction will scale accordingly. In other words, if we can control the amount of exogenous promotions, we could boost or suppress the number of views for videos that respond to such promotions.
- *Shifting in time:* if the exogenous stimuli is shifted in time, so will the views responding to it. In other words, we could schedule promotions (and subsequent views) for videos that respond to such promotions.

The *sliced* fitting graph in Figure 2 of the main text can be understood as an illustration of these three properties. In reality we observe the exogenous stimuli $s(t)$ as a discretized function (denote discrete time index as $[t]$) consisting a series of impulses located at $\tau = 1, 2, \dots, T$, i.e.

$$\sum_{\tau=0}^T s[\tau] \delta[t - \tau] \quad [22]$$

Directly following from the three properties, we can see that $\xi[t]$ is a superposition of impulse response function $\hat{\xi}[t]$ scaled by $s[\tau]$ and shifted by the corresponding amount, i.e.

$$\xi[t] = \sum_{\tau=0}^T s[\tau] \hat{\xi}[t - \tau] \quad [23]$$

2 Fitting the Hawkes intensity model

This section describes some of the implementation and computational details for estimating the model in Eq 20 from observed popularity and promotion histories.

2.1 Settings for model estimation. We first present the view of Eq 20 over data obtained in discrete time intervals, and then discuss a way to estimate missing external influence, and finally list the loss function for least-squares fitting.

Discretizing over time Behavioral statistics are aggregated and presented over fixed, discrete, intervals – in the case of YouTube, we observe the daily history of views $\xi[t]$ and shares $\bar{s}[t]$ for $t = 1, \dots, T$. Writing Eq 20 over discrete time, we obtain:

$$\xi[t] = \mu s[t] + C \sum_{\tau=1}^t \xi[t - \tau] \hat{\tau}^{-(1+\theta)} \quad [24]$$

Hereafter, we use square brackets to denote discrete time (e.g. $s[t], \xi[t]$) and round brackets to denote continuous time (e.g. $s(t), \xi(t)$).

Accounting for unobserved external influence. In addition to observed external promotions $\bar{s}[t]$ in tweets or shares, we model unobserved external excitation as an initial shock (at $t = 0$) and a constant background excitation (for $t > 0$).

$$s[t] = \frac{\gamma}{\mu} \mathbb{1}[t = 0] + \frac{\eta}{\mu} \mathbb{1}[t > 0] + \bar{s}[t] \quad [25]$$

where $\mathbb{1}(arg)$ takes the value 1 when arg is true and 0 otherwise. In the absence of a parametric temporal model of generic external influence, the initial impulse and constant components require the least amount of assumptions about how unobserved influence evolve. In our experiments, adding estimates for such unobserved influence components improves the fitting for a large number of videos.

The loss function For each video with observed $\{\xi[t], \bar{s}[t], t = 1, \dots, T\}$, we find an optimal set of models parameters $\{\mu, \theta, C, c\}$ and also estimate the unobserved external influence (parameters γ and η). This is done by minimizing the square error between the series $\xi[t]$ and the model $\hat{\xi}[t]$, $\forall t \in 0, 1 \dots T$. The corresponding optimization problem is as follows:

$$\begin{aligned} \min_{\mu, \theta, C, c, \gamma, \eta} J &= \frac{1}{2} \sum_{t=0}^T (\xi[t] - \hat{\xi}[t])^2 \\ \text{Eq. 24} &= \frac{1}{2} \sum_{t=0}^T \left(\gamma \mathbb{1}[t = 0] + \eta \mathbb{1}[t > 0] + \mu \bar{s}[t] \right. \\ &\quad \left. + C \sum_{\tau=1}^t \xi[t - \tau] \hat{\tau}^{-(1+\theta)} - \hat{\xi}[t] \right)^2 \\ \text{s.t. } &\mu, \theta, C, c > 0 \end{aligned} \quad [26]$$

Note that Eq 26 involves the model components $\xi[t - \tau]$ – as we will show in the next sub section, the objective function and its gradients are computed iteratively by estimating $\xi[\tau]$ from $\xi[1], \dots, \xi[t - 1]$. Also note that the recursive term is model estimates $\xi[t - \tau]$ rather than observations $\hat{\xi}[t - \tau]$, as we would like to have the model reproducing the whole observed time series, rather than predicting the next point given observed history. As will be discussed in SI. Sec. 2.3, we further improve fitting stability by adding a \mathcal{L}^2 regularizer to the objective function.

2.2 Computing gradients. Eq. 26 is a non-convex objective, we use gradient-based optimization approach, and specifically L-BFGS [9] with pre-supplied gradient functions. We use the implementation supplied with the NLOpt package [7]. We fit each video in parallel, starting with multiple random initializations to improve solution quality, and we present the solution with the lowest error function J . The gradient computations are listed as follows.

We define the error term as $e[t] = \xi[t] - \bar{\xi}[t]$, Eq 26 now becomes $J = \frac{1}{2} \sum_{t=0}^T e^2[t]$. Since $\xi[t]$ are observed quantities,

$$\frac{\partial e[t]}{\partial var} = \frac{\partial \xi[t]}{\partial var},$$

where $var \in \{\mu, \theta, C, c, \gamma, \eta\}$. Using chain rule, we obtain:

$$\frac{\partial J}{\partial var} = \sum_{t=0}^T e[t] \frac{\partial \xi[t]}{\partial var} \quad [27]$$

Specifically, we compute the following partial derivatives and use them in Eq 27 to compute the gradient.

$$\frac{\partial \xi[t]}{\partial \mu} = \begin{cases} \bar{s}[t] + C \sum_{\tau=1}^t \frac{\partial \xi[t-\tau]}{\partial \mu} (\tau + c)^{-(1+\theta)} & , t > 0 \\ \bar{s}[0] & , t = 0 \end{cases} \quad [28]$$

for $t > 0$,

$$\begin{aligned} \frac{\partial \xi[t]}{\partial \theta} &= C \sum_{\tau=1}^t \frac{\partial \xi[t-\tau]}{\partial \theta} (\tau + c)^{-(1+\theta)} \\ &\quad + \xi[t-\tau] \frac{\partial}{\partial \theta} (\tau + c)^{-(1+\theta)} \\ &= C \sum_{\tau=1}^t \left[\frac{\partial \xi[t-\tau]}{\partial \theta} - \xi[t-\tau] \ln(\tau + c) \right] (\tau + c)^{-(1+\theta)} \end{aligned} \quad [29]$$

for $t = 0$, $\frac{\partial \xi[0]}{\partial \theta} = 0$.

for $t > 0$,

$$\frac{\partial \xi[t]}{\partial C} = \sum_{\tau=1}^t C \frac{\partial \xi[t-\tau]}{\partial C} (\tau + c)^{-(1+\theta)} \quad [30]$$

$$+ \xi[t-\tau] (\tau + c)^{-(1+\theta)} \quad [31]$$

for $t = 0$, $\frac{\partial \xi[0]}{\partial C} = 0$.

for $t > 0$,

$$\begin{aligned} \frac{\partial \xi[t]}{\partial c} &= C \sum_{\tau=1}^t \frac{\partial \xi[t-\tau]}{\partial c} (\tau + c)^{-(1+\theta)} \\ &\quad - (1 + \theta) \xi[t-\tau] (\tau + c)^{-(2+\theta)} \end{aligned} \quad [32]$$

for $t = 0$, $\frac{\partial \xi[0]}{\partial c} = 0$.

For the unobserved external stimuli γ and η .

for $t > 0$,

$$\frac{\partial \xi[t]}{\partial \gamma} = C \sum_{\tau=1}^t \frac{\partial \xi[t-\tau]}{\partial \gamma} (\tau + c)^{-(1+\theta)} \quad [33]$$

for $t = 0$, $\frac{\partial \xi[0]}{\partial \gamma} = 1$.

for $t > 0$,

$$\frac{\partial \xi[t]}{\partial \eta} = 1 + C \sum_{\tau=1}^t \frac{\partial \xi[t-\tau]}{\partial \eta} (\tau + c)^{-(1+\theta)} \quad [34]$$

for $t = 0$, $\frac{\partial \xi[0]}{\partial \eta} = 0$.

Note that the gradient computation is iterative, i.e. the computation of $\frac{\partial \xi[t]}{\partial var}$ makes use of $\frac{\partial \xi[\tau]}{\partial var}$ for $\tau = 1, \dots, t-1$.

2.3 Adding an \mathcal{L}^2 regularizer. We add \mathcal{L}^2 regularization on the linear coefficients of the Hawkes Intensity Process to avoid overfitting. The loss function with the regularization terms are as follows.

$$J_{reg}(\omega, \mu, \theta, C, c) = J(\mu, \theta, C, c) + \frac{\omega}{2} \left(\left(\frac{\gamma}{\gamma_0} \right)^2 + \left(\frac{\eta}{\eta_0} \right)^2 + \left(\frac{\mu}{\mu_0} \right)^2 + \left(\frac{C}{C_0} \right)^2 \right), \quad [35]$$

Here $(\gamma_0, \eta_0, \mu_0, C_0)$ are reference values for parameters obtained by fitting the series $\bar{\xi}[t]$ without regularization. The reference values are used to normalize the parameters in the regularization process, so that they have equal weights. Intuitively using \mathcal{L}^2 normalization in square-loss is effectively putting a Gaussian prior on the parameters being regularized. We desire parameters c and θ to take values away from zero, hence they are not regularized. The \mathcal{L}^2 regularization term is differentiable with respect with variables (γ, η, μ, C) and the terms $\frac{\omega}{\gamma_0}$, $\frac{\omega}{\eta_0}$, $\frac{\omega}{\mu_0}$ and $\frac{\omega}{C_0}$ are added respectively to the RHS of Eq. 33, 34, 28 and 30.

The regularizer parameters ω is expressed as a percentage of J_0 (the value of the non-normalized error function) and it is determined through a line search within $[10^{-4}J_0, 10J_0]$ in log-scale. ω is tuned per video, on a temporally hold-out tuning sequence, i.e. we use the first 75 days of observed popularity for parameter estimation, the next 15 days for tuning ω , and day 91-120 for forecasting popularity.

3 Data

We construct a "Tweeted Videos" dataset using the data APIs from both Twitter and YouTube. We stream tweets from Twitter API using a set of keywords related to YouTube and its videos. This returns over 5 million matched tweets per day after URL expansion and tokenization performed by Twitter, most of which mention and link to a YouTube video. The raw dataset used in this study was from 2014-05-29 to 2014-12-26, having 1,061,661,379 tweets in total. From each of these tweets, we extracted the associated YouTube video id (only the first in case multiple videos were referenced in the same tweet), resulting in 81,915,174 distinct videos in total.

From YouTube.com, we obtained video metadata including its upload date and video category, as well as the time series consisting daily number of views and shares. Along with the daily number of tweets, we obtained three attention-related time series for each video: $(views[t], shares[t], tweets[t])$, here t indexes time with unit of a day. For the number of views and shares, the time range is from the video's upload date to the data collection (i.e. February-March 2015). For number of tweets, time ranges from the videos upload date or 2014-05-29 (whichever is later) to 2014-12-26.

3.1 The 5Mo and ACTIVE datasets. We constructed two cleaned data subsets from the feed of tweeted videos, in order to collect basic data statistics and estimate the model.

- The 5Mo was constructed to have videos whose popularity history is at least 60 days long, and is used for forecasting popularity. We narrow down the timeframe of video upload to between 2014-05-29 and 2014-10-24 in order to have long enough history. There are 16,417,622 videos with publicly-available popularity history. We did not obtain the popularity history for more than half of the videos, reasons

for such data loss include: a video is no longer online, a video’s popularity history is not publicly-available, or requests that resulted in web server errors. This large and diverse sample allows us to estimate the background statistics of video views, tweets, and shares, as will be discussed in the next subsection.

- The ACTIVE dataset selects videos uploaded between 2014-05-29 and 2014-08-09 and which have received at least 100 tweets and at least 100 shares during recorded lifetime. The timeframe is selected to ensure that each video has at least 120 days of tweeting and popularity history in our dataset, the activity threshold is used to ensure there is sufficient data for estimating the Hawkes intensity model and producing a forecast as describe in Section 5. Table 1 presents the category distribution for the ACTIVE dataset. It is noteworthy that the largest 4 categories cover more than 70% of all the videos in ACTIVE, with more than 25% of the videos being **Music**. We removed 6 content categories (i.e. **Autos & Vehicles**, **Travel & Events**, **Pets & Animals**, **Shows**, **Movies**, **Trailers**) containing less than 1% of the videos in the dataset. Their corresponding videos were also removed. The resulting dataset contains 13,738 videos.

Table 1: Number of videos broken down by category in the ACTIVE dataset. **Music** represents a significant proportion (25%) of all the videos.

Category	#vids	Category	#vids
Comedy	865	Music	3549
Education	298	News & Politics	1722
Entertainment	2422	Nonprofits & Activism	333
Film & Animation	664	People & Blogs	1947
Gaming	882	Science & Technology	262
Howto & Style	180	Sports	614
Total:	13,738		

3.2 The popularity scale over time. It is well-known that network measurements such as the number of views follows a long-tailed distribution. To facilitate discussions about popularity and attention, we propose to quantify popularity on an explicit percentage scale, with 0.0% being the least popular, and 100% being the most popular. Videos are grouped into *Popularity Bins* by viewcounts that they receive at t days after upload, and each bin $\xi_t(k)$ is marked with its maximum popularity percentile – videos in bin k are at most among the top $k\%$ popular with age t . In this work we use 40 evenly spaced bins, i.e., $k = 2.5, 5.0, 7.5, \dots, 100$, and each bin contains 2.5%, or $\sim 41K+$ videos for 5Mo.

Figure 1(a) and (b) contains a boxplot of video viewcounts (in log-scale) of each bin after 30 and 60 days, respectively. We can see the long tailed distribution of popularity in YouTube reflected here – videos in the less popular bins have very similar number of views, e.g. the first 6 bins, or 15% of the videos, all have less than 10 views; videos in each the middle bins (e.g. $k = 17.5, \dots, 85.0$) are within 1.5 times of the view count of each other; yet viewcounts of the 5% most popular ($k = 97.5$ and $k = 100$) videos span over almost two orders of magnitude. For videos in 5Mo after their first 30 and 60 days of upload, the shape of the overall popularity scale remains the same, with a slight increase in the dynamic range of views (top of the last boxplot). The popularity scale of the ACTIVE is very similar to the one presented in Figure 1(a) and (b), the only notable difference being the number of views corresponding to each bin. ACTIVE is a subset of the most popular videos, as shown by Figure 2: the videos in ACTIVE are positioned in the top 5% popularity percentiles of 5Mo ($k = 97.5$ and $k = 100$).

In Figure 1(c) we explore the change of popularity of each video from 30 days (y-axis) to 60 days (x-axis). Note that most videos retain a similar rank (in the boxes along the 45 degree diagonal line), or have a slight rank decrease as they are overtaken by other videos (slightly above the diagonal in the plot). No outliers exist in the upper-left part of the graph, since a video cannot lose viewcount that it already gained. Most notably, we can see that video from any bucket can *jump* to the top popularity buckets between 30 and 60 days of age, such as the outliers for the few boxes on the far right. This phenomenon elicits important questions: how did these videos do viral, and whether or not it is related to external promotions.

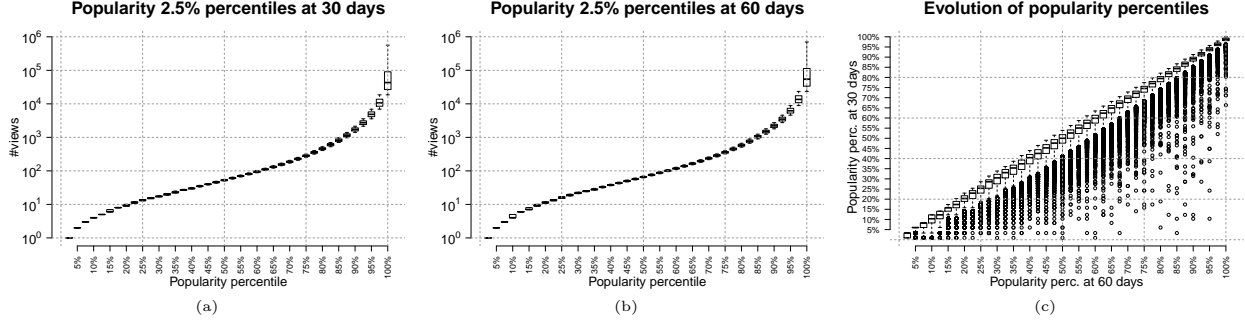


Figure 1: The popularity scale of YouTube videos in the 5MO dataset. The total number of **views** obtained by each video in the first 30 days (a) and 60 days (b) after upload is divided into 40 equally spaced bins (i.e. each with 2.5% of the videos). The 2.5% most popular videos span almost two orders of magnitude in views. Note that outliers in this bin are not represented, as the most popular videos in the collection have $\sim 10^8$ views. (c) Evolution of popularity between 30 and 60 days. The outliers are videos that have improved significantly on the popularity scale.

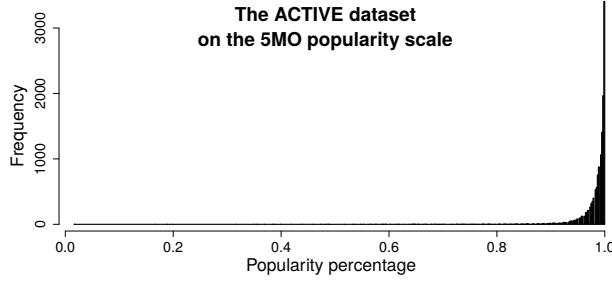


Figure 2: Positioning of the ACTIVE dataset on the popularity scale of the 5MO dataset (at 30 days after upload). The horizontal axis shows the popularity percentiles in the 5MO dataset, while the vertical axis shows the corresponding frequency of videos in ACTIVE. Visibly, ACTIVE is a subset of the most popular videos in 5MO.

4 Understanding popularity dynamics

In this section, we provide additional observations on parameters of the Hawkes intensity model, supplementing the analysis presented in the main text Section “What describes the most popular videos”. Specifically, we relate the distribution of specific parameter values such as memory exponent or exogenous sensitivity, to video groups – channels, content categories – and a video’s popularity.

4.1 Behavior across groups of videos: categories and channels. We provide in this subsection some observations on behavior statistics and key parameters broken down by video

category. Furthermore, we show how the endo-exo map can be used to detect consistent behaviors across YouTube channels.

Consistent behavior across channels We use the endo-exo map to visualize groups of videos that belong to the same user-assigned content type, or are from the same author, called *channel* in YouTube. Fig. 3 shows a scatter plot of videos posted by a reporter in category **News & Activism** (in red) and a user focusing on recordings of **Game** sessions (in blue). The game recording videos are generally more popular (bigger circles) than the news videos, and this is explained by the former group having higher exogenous sensitivity – higher values of μ .

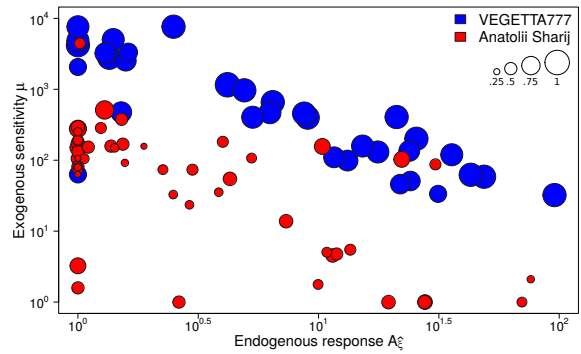


Figure 3: Video channels on the endo-exo map. Scatter plot of videos from a reporter covering events in Ukraine (Anatolii Sharij, in red) and Spanish game recording videos channel (VEGETTA777, in blue). Radii of the circles are proportional with the popularity percentile of each video.

The effect of the external influence is not equal. We examine the amount of attention (in number of views) and external influence (in number of shares and tweets) in the ACTIVE dataset. This provides a basis for understanding the corresponding Hawkes intensity model. Figure 4 (top row) contains box plots of total views, along with total shares and tweets, broken down by video category. The left-most boxes (in red) depicts the profile of all videos. One notable example is videos in the **Nonprofits & Activism** category: overall they have less-than-average amount of views, despite being shared more than the median number of times.

Observed versus unobserved external influences. Model parameters γ and η can be interpreted respectively as the initial impulse and constant exogenous stimuli not captured in the observed exogenous activity $s(t)$. From the bottom left two plots in Figure 4, we can see that several categories have significantly higher components of γ and η , such as **Gaming**, **Comedy** and **Entertainment**. This may result from a significant volume of activity outside of Twitter or Youtube sharing – **Gaming** videos, for example, is known to spread on dedicated social networks such as sub-reddit [/r/gaming/](#), [/r/gamingvids/](#) or forums, such as [www.minecraftforum.net](#).

Exogenous sensitivity and endogenous response. The two bottom right plots of Figure 4 represent the breakdown per category of, respectively, the exogenous sensitivity μ and the endogenous response $A_{\hat{\xi}}$. These plots present an alternative view to the 2-dimensional density distribution of each category on the *endo-exo map*, shown in Figures 10 and 11. Certain categories, such as **Comedy**, **Gaming** or **Sport** seem to be particularly sensitive to external influence. Categories like

Comedy, **Entertainment** or **Gaming** observe higher than median endogenous responses. The fact the **Comedy** and **Gaming** show both a high exogenous sensitivity and endogenous response provide a plausible explanation to why these categories observe relative high popularity (**#views**) despite their relative low sharing. Conversely, **Nonprofits & Activism** exhibits lower than median values for both μ and $A_{\hat{\xi}}$ which accounts for its low popularity (even though highly shared).

Categories of longer versus shorter memory. Figure 5 plots distributions of the memory exponent θ , obtained using kernel density estimation. θ value for three categories, **Music**, **Nonprofits & Activism** and **News & Politics** (in red) are contrasted with the distribution from **All** videos (in blue). The solid lines in each graph indicate the median value for θ in each category, whereas the dashed lines indicate the mean value. All video categories, as well as the general population, observe a long tail distribution for θ , with a peak density around $\theta \simeq 3.35$. A small θ leads to slower decay over time (and larger endogenous response $A_{\hat{\lambda}}$), whereas a large θ means an event is *forgotten* quickly (i.e. small $A_{\hat{\lambda}}$). We can see that a larger (than random) fraction of **Music** videos decay slowly ($\text{mean}_{\theta, \text{all}} = 15.94$, $\text{mean}_{\theta, \text{music}} = 14.95$), while more **News & Politics** and **Nonprofits & Activism** videos are forgotten faster, with $\text{mean}_{\theta, \text{nonprofit}} = 17.56$ and $\text{mean}_{\theta, \text{news}} = 19.45$. This suggests that there is a systematic difference across different types of videos in the rate at which the collective *memory* decays – one explanation for such differences can be that music is typically considered *timeless* content while news is considered *timely* whose relevance decreases rapidly over the first few days.

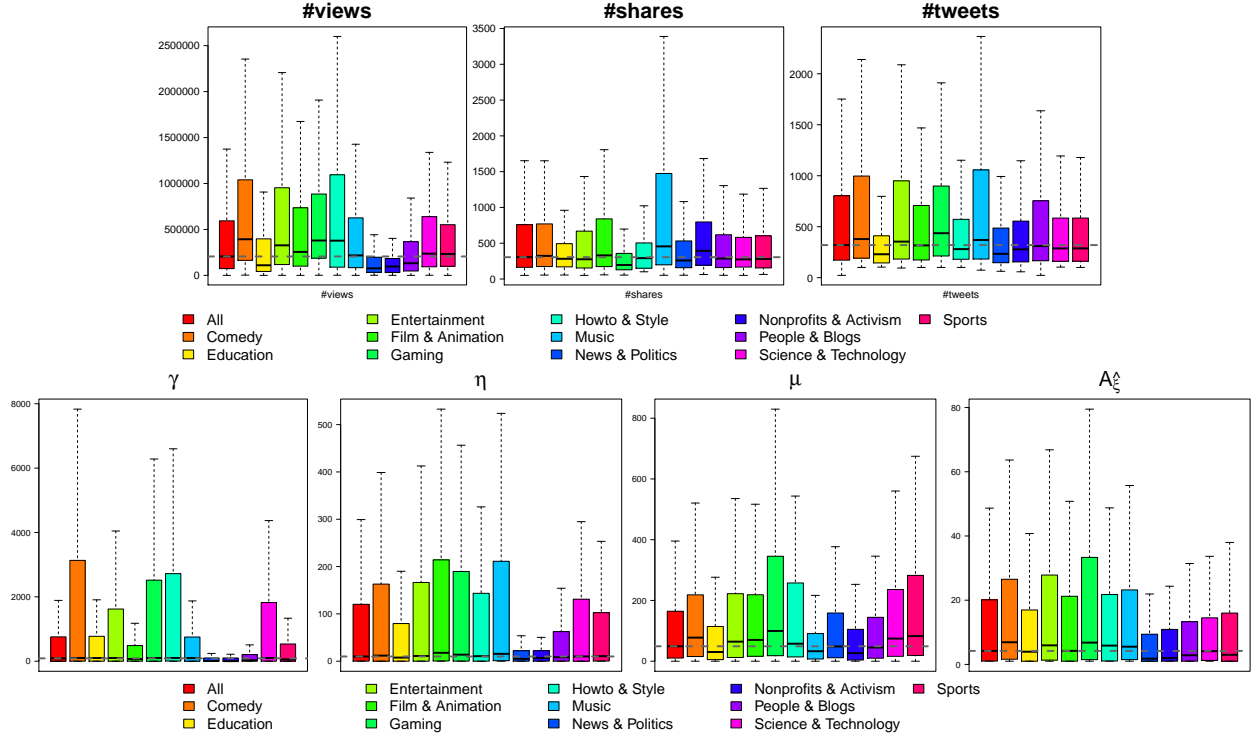


Figure 4: (Top row) The number of views (left), shares (center) and tweets (right) for videos in different categories. (Bottom row) Box plots of unobserved exogenous influence (initial impulse γ , constant excitation η), exogenous sensitivity μ and endogenous response A_{ξ} , broken down by category.

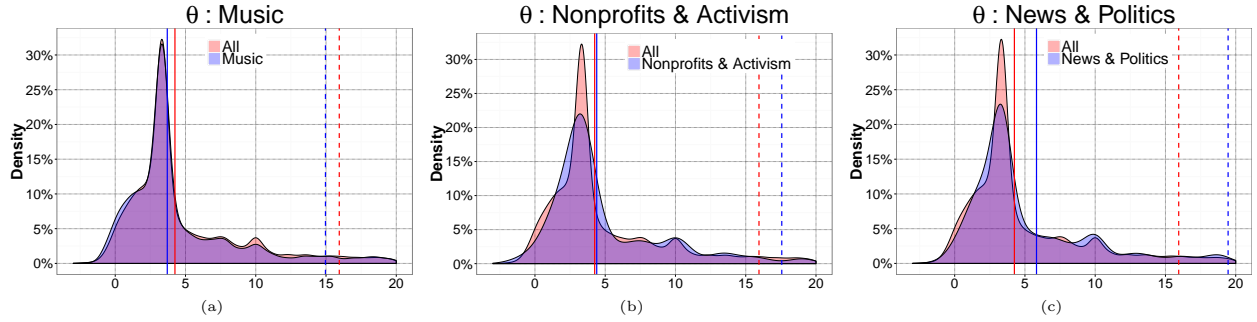


Figure 5: Distribution of the memory exponent θ for 3 categories: Music (a), Nonprofits & Activism (b) and News & Politics (c), compared to the background distribution in all videos. Solid vertical lines indicate the median θ value in each population, whereas the dashed vertical lines indicate the mean θ . Color of lines corresponds to legend.

4.2 What makes videos popular. In this section, we provide additional details about the relation between video popularity and fitted values of parameters μ and θ . These analyses provide additional details to the endo-exo map, by explicitly linking the endogenous and exogenous components of each video to each model parameter.

Parameters μ and θ and popularity In the Main Text, we claim a direct connection between μ the exogenous sensitivity and popularity and an inverse connection between the θ the time-decay rate of the memory kernel and the popularity. We provide, in Fig. 6, empirical proof of these connections by studying the popularity distribution for low and high values of the above parameters. The top-left graphic shows the density distribution of the fitted values of μ in the ACTIVE dataset. There is a high peak of density around $\mu = 1$, corresponding to videos with low sensitivity to external influence, and a second peak around $\mu = 10^{1.73} = 53.7$, corresponding to videos with higher exogenous sensitivity. We divide the range of μ into deciles (groups of 10% each) and we select the second decile (i.e. low sensitivity) and the tenth decile (high sensitivity), hashed in gray on the graphic. In the bottom-left graphic, we plot the popularity distribution for videos within each of the above deciles of μ . The subpopulation of videos with low exogenous sensitivity show a dense area of low popularity, and with only very few videos making it into the top popularity percentiles. Conversely, the density distribution of the subpopulation of videos with high exogenous sensitivity shows an increasing trend, with a concentration of highly popular videos. This confirms the intuition that highly popular videos tend to have high values of exogenous sensitivity μ .

Similar results can be shown for the time-decaying memory exponent θ , which controls how fast videos are forgotten and the size of the endogenous response $A_{\hat{\lambda}}$. Fig. 6b plots the density distribution of θ , which shows a peak at $\theta = 3.36$ and selects the second and tenth percentile, corresponding respectively to low values and high values of θ . Similarly to

μ , the bottom-center graphic plots the popularity distribution for each of the subpopulations defined by the selected deciles of θ . The subpopulation with high values of θ (i.e. low $A_{\hat{\lambda}}$) tends to be forgotten more quickly and shows a concentration of videos with low popularity, whereas videos with lower values of θ (and higher $A_{\hat{\lambda}}$) tend to be more popular.

Endo-exo map for additional categories. The above considerations are at the basis of the construction of the *endo-exo map*, as shown in the Main Text and its potentially viral region – videos with high values of both exogenous sensitivity μ and endogenous response $A_{\hat{\lambda}}$ are more susceptible to become popular *if given the required attention*. The right column of Fig. 6 plots the 2D density of videos on the endo-exo map for the entire ACTIVE dataset (top) and the top 5% most popular videos (the color map is aligned for the two graphics). Visibly, the distribution of the popular videos is skewed towards the more viral region of the map (i.e. high μ and high $A_{\hat{\lambda}}$). In Fig. 10 and 11, we repeat this analysis and we further break down the ACTIVE population, based on video category. We plot pairs of 2D densities of videos on the endo-exo map for all categories, except Gaming and Film & Animation, which were discussed in the Main Text Fig. 3. This visually reveals some of the dynamics that propel videos to the most popular segment, in each subpopulation. For example, categories like Gaming, Science & Technology Travel & Events have the distribution of the most popular videos shifted top-right w.r.t to rest of the category (similar to the dynamics shown for the entire population). Other categories appear only upward-shifted (i.e. only higher μ) w.r.t to rest of the category: Film & Animation, Entertainment, Howto & Style, News & Politics and People & Blogs. There is even an outlier category, Comedy, which seems to have two heat centers in the top 5% popular subpopulation. This seems to indicate two distinct patterns of becoming popular within this category: one pattern involves being sensitive to exogenous excitation more than the average video, whereas the second pattern involves higher endogenous propagation in the network (higher $A_{\hat{\lambda}}$).

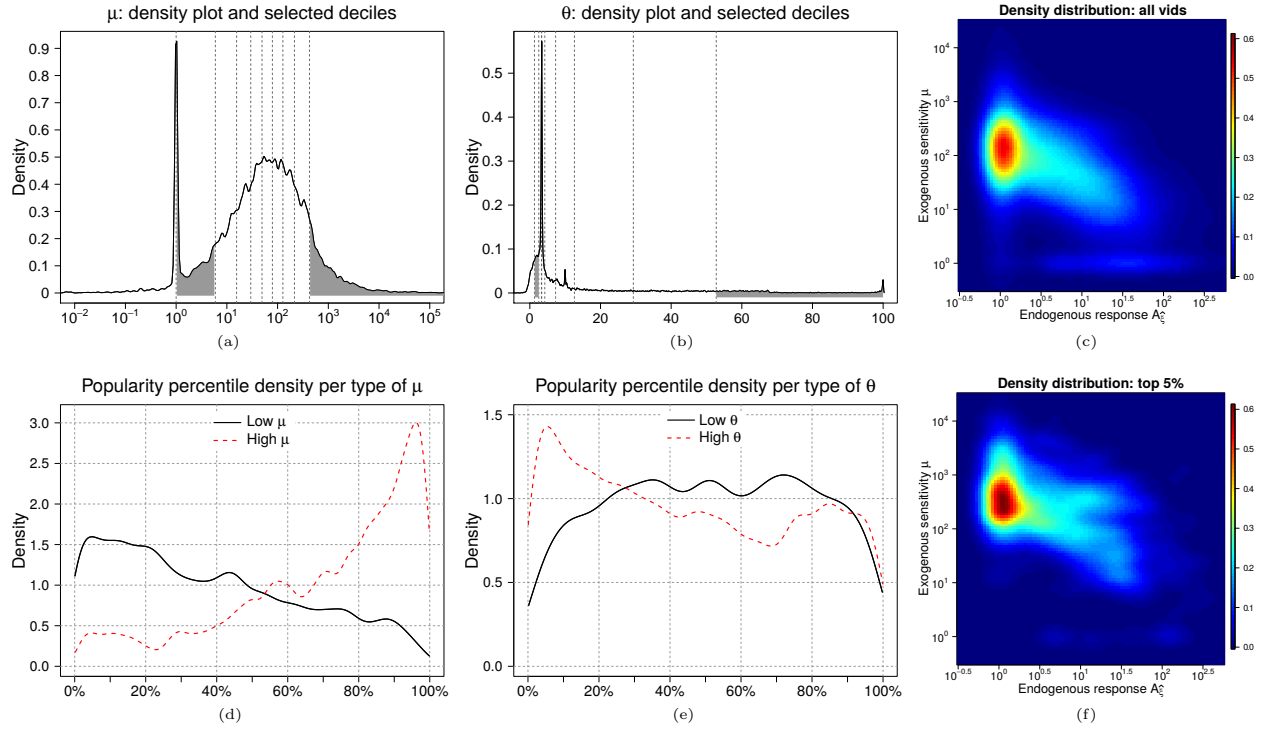


Figure 6: Density distribution of fitted model parameters values μ (left column) and θ (center column). The range of each fitted parameter is divided into 10 deciles, shown by vertical dotted gray lines (in the top row). For each of parameters μ and θ , 2 deciles are chosen (one corresponding to high values, and a second one corresponding to low values), shown shaded in gray. For each parameter, the bottom row plots the popularity distribution for videos within each of the chosen deciles. Right column: the *endo-exo* map 2 dimensional density distribution for all videos (top) and top 5% most popular videos (bottom). The density distribution of most popular videos is skewed towards the more viral area of the map (high μ and high A_ξ).

Table 2: Granger causality test: number of videos in the ACTIVE set for which the null hypothesis (i.e. absence of Granger causality) is rejected with $p < .001$. The left side of the table shows the number of videos for which an unidirectional Granger causality is detected – i.e. for 114 videos tweets Granger-cause shares and not the other way around. The right side shows the number of videos for which the relation is detected in both directions. Note that when a video presents a bidirectional relation, it is not counted the unidirectional relations for the same pair of series.

	unidirectional			bidirectional		
	tweets	shares	views	tweets	shares	views
tweets	-	114	164	-	22	18
shares	136	-	537	-	-	253
views	162	833	-			-

4.3 Causal connection between the views, tweets and shares series.

In this section, we investigate the causal connection between the series of views, shares and tweets, for each of the videos in the ACTIVE dataset. We test for causality using time-series analysis tools. We employ a F-type Granger-causality test [4], implemented in the R package `vars` [12]. For each series of each video we construct a Vector Autoregressive Model, with the lag determined automatically using minimal AIC. Next, we perform a Granger causality test for each video and each pair of temporal series – i.e. (views, shares), (views, tweets) and (tweets, shares). Each test is performed in both directions – e.g. views Granger-cause shares and shares Granger-cause views. The null hypothesis is that no causal relation exists between the series. We reject the null hypothesis and we accept the existence of a causal relation when we observe a test p-value lower than 10^{-3} .

Table 2 shows the number of pairs in each setup for which the causal relation is considered to be significant. Note that the causal relation can be reciprocal – e.g. for 253 videos, both the shares Granger-cause the views and the views

Granger-cause the shares. Considering the scale of the ACTIVE dataset (around 14 thousands videos), a causal relation is detected for no more than 6% of the videos – i.e. for the relation views Granger-cause shares, true for 833 videos. For all pairs of series, the number of videos presenting a unidirectional relation seems comparable (e.g. tweets Granger-cause views for 164 videos, and shares Granger-cause tweets for 162 videos). We cannot identify a clear Granger causality relation between different series. As there does not yet exist a standard method for capturing non-linear causal relationships or causality with confounding effects, we leave this as future work.

5 Popularity forecasting and comparison to baseline

In this section we provide additional details and results to complete the Main Text Sec. “Forecasting popularity growth”, namely, more information about the performance break down of different approaches and the statistical testing analysis for detecting statistically significant differences in the forecasting performance.

The series of the first 90 days of each video history in ACTIVE dataset are used to fit the Hawkes intensity model parameters. The series is divided into two sub-series: the first 75 days are used to fit parameters $\{\mu, \theta, C, c\}$, while the last 15 days for the holdout series used to fit the regularizer meta-parameter ω . Either **#shares** and **#tweets** series can serve as the known exogenous stimuli series $s(t)$. The Multi-Linear Regression (MLR) [13] baseline is trained using the same data. We adapt the original algorithm by predicting the value of the viewcounts for each of the 30 days between day 91 and 120. Furthermore, we build an enhanced version (denoted by *MLR (#shares)* or *MLR (#tweets)*) by introducing the exogenous influence as additional variables, both in the training and in the prediction. The baseline is particularly sensitive to outliers, which we remove from the training set. A video is considered an outlier if it has received a large burst of views in the period from 91 to 120 days. More precisely, we remove any video having received twice as many view between days 91 and 120 than then do between 61 and 90. 3.5% of the videos are considered outliers and eliminated from the training set. The errors are measured in average error in popularity percentile, as defined in the main text.

5.1 Additional results. In addition to the performance comparison, shown in the Main Text Fig. 4, Figure 8 (a) presents the Cumulative Distribution Function (CDF) of the prediction errors for the Hawkes intensity model, MLR and MLR (**#shares**). The Hawkes intensity model consistently outperforms MLR (with and without the exogenous stimuli information): the Hawkes model forecasts popularity of 87% of the video population with a maximum 10% error, while MLR covers only 78% of the population for the same error threshold. Furthermore, MLR (**#shares**) obtains only marginal performance improvements over MLR, even while using the exogenous information. Figure 8 (b) shows the absolute forecasting error performances, aggregated using barplots. Visibly, the Hawkes intensity model (using either **#shares** and **#tweets**) consistently outperforms MLR both in term of median values and variation, which results in the better mean values of forecasting error already shown in the Main Text Fig. 4 (center). Figure 8 (c) analyzes closely the forecasting error distribution for the best performing version of each approach. The Hawkes (**#shares**) blue curve shows a concentration of lower errors and a median error value of 3%. The red curve corresponds

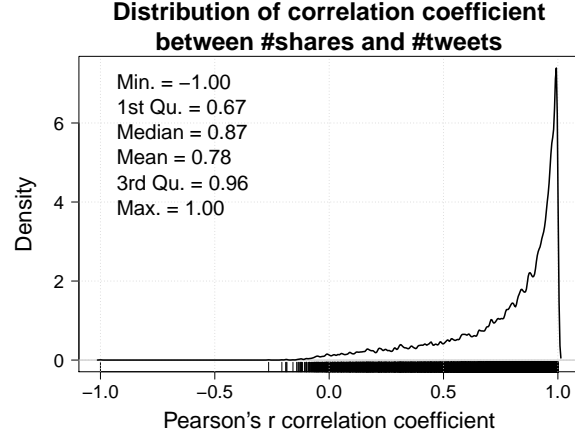


Figure 7: Density distribution of Pearson’s r correlation coefficient between **#shares** and **#tweets** for each video in the ACTIVE dataset. The legend values give the quartiles and the mean of the obtained coefficients.

to the error distribution for the MLR (**#shares**) and shows a higher concentration of larger error and a median error value of 3.75%.

5.2 Statistical significance. We study the statistical significance of the difference of performance in forecasting popularity, observed in main text Fig. 4(b). We break down the study into two questions: 1) is the difference of forecasting performance between the Hawkes intensity process and the MLR baseline statistically significant? and 2) does the source of exogenous stimuli – **#shares** or **#tweets** – influence the quality of the forecasting? We setup four experiments: two experiments comparing the performances of forecasting methods for each of the two sources of influence and two experiments comparing the effect of the sources for each of the two algorithms. Based on the selected setup, we construct two samples and we perform a T-test. For each experiment, the null hypothesis assumes that the mean of two samples are equal (i.e. there is no difference in forecasting performance). The alternative hypothesis assumes that the true means of two samples are not equal.

Statistical testing with large sample size

The well-known p -value issued from hypothesis testing is dependent on the observed difference between the two samples, as well as the sample size. This renders analyses based only on p -value particularly sensitive to sample size, given that with sufficiently large samples, a statistical test will almost always demonstrate a significant difference [14]. Given the size of the ACTIVE dataset (i.e. 13,738) which serves as sample for the four experiments hereafter, we measure the *effect size* in addition to the typical p -value. The effect size measure which we report and we use to justify our analysis is *Cohen’s d coefficient* [2], defined as the difference of the means scaled by the inverse of the standard deviation of both populations

Experimental setup

Our forecasting systems uses two inputs: the observed **#views** and an external stimuli source (either **#shares** or **#tweets**). Answering question 1) – significance of performance difference between the Hawkes intensity model and the MLR baseline

Table 3: Summary of statistical test on the forecasting performance differences. Each line corresponds to a performed T-test, either comparing two exogenous sources or two forecasting algorithms. Columns “Sample A” and “Sample B” describe the two compared samples in terms of used algorithm and exogenous source, mean value and standard deviation. The first two tests are *two sample T-tests*, whereas the last two lines correspond to *paired T-tests* (more details about the underlying rationale in the text). M denotes sample mean, SD standard deviation.

Exogenous source	Forecasting algorithm	Sample A	Sample B	T-test p-val	Cohen’s d
#shares vs. #tweets	Hawkes	Hawkes (#shares) $M = 4.96 \times 10^{-2}, SD = 6.3 \times 10^{-2}$	Hawkes (#tweets) $M = 5.35 \times 10^{-2}, SD = 6.88 \times 10^{-2}$	6.83×10^{-7}	-0.05
#shares vs. #tweets	MLR	MLR (#shares) $M = 6.94 \times 10^{-2}, SD = 9.08 \times 10^{-2}$	MLR (#tweets) $M = 6.94 \times 10^{-2}, SD = 9.05 \times 10^{-2}$	0.98	0.00
#shares	Hawkes vs. MLR	Hawkes (#shares) $M = 4.96 \times 10^{-2}, SD = 6.3 \times 10^{-2}$	MLR (#shares) $M = 6.94 \times 10^{-2}, SD = 9.08 \times 10^{-2}$	8.57×10^{-151}	0.253
#tweets	Hawkes vs. MLR	Hawkes (#tweets) $M = 5.35 \times 10^{-2}, SD = 6.88 \times 10^{-2}$	MLR (#tweets) $M = 6.94 \times 10^{-2}, SD = 9.05 \times 10^{-2}$	2.41×10^{-95}	0.197

– boils down to comparing two treatments to a single set of individuals. This translates into applying a *paired T-test* to a single sample. Conversely, comparing the two sources of exogenous excitation involves applying the same forecasting method to two different populations. This leads to applying a *two-sample T-test*.

No performance difference between the two exogenous stimuli sources

The detailed results of each of the four hypothesis testings are presented in Table 3. The first two lines correspond to the two-sample T-tests, dealing with the difference between the two sources of exogenous stimuli. The first test uses the Hawkes intensity model as forecasting algorithm, the second one uses the MLR baseline. For both tests, the Cohen’s d coefficient has a negligible value. This suggests that no significant difference exists when forecasting future popularity using #shares or #tweets as external stimuli. The very small p-value yielded in the first test ($\sim 10^{-7}$) is most likely an artifact of the large sample size. These two results indicate that the same forecasting performance is achieved using either source of external stimuli, regardless of the forecasting algorithm. Furthermore, a correlation analysis between the two sources reveals the same conclusion: for each video we compute the Pearson’s correlation coefficient between the two time series #shares and #tweets. Fig. 7 shows the density distribution of the correlation coefficient. Visibly, the two series are highly correlated for most videos.

Significant difference between the Hawkes model and MLR

The last two lines of Table 3 show the results of testing the performances of the Hawkes intensity model against the baseline, for each of the two external sources. In both cases, the Cohen’s d coefficient shows a small, but nonnegligence effect size. Together with the very low p-values ($\sim 10^{-151}$ for #shares, $\sim 10^{-95}$ for #tweets), this makes us reject the null hypothesis and conclude that the differences between the two forecasting methods are statistically significant.

5.3 Forecasting performance on difficult videos. The difference of forecasting performance is even more noteworthy for more *difficult* videos – those that present a large exogenous shock in the forecasting period (a real example of such a video is depicted in Figure 9 (a)). A video is considered to present a high exogenous shock if the exogenous stimuli series $s(t'), t' \in \text{TEST}$ contains at least one point t' so that $s(t') > \text{mean}(s(t^*)) + 10\text{var}(s(t^*))$, with $t^* \in \text{TRAIN}$. 4006 videos in the ACTIVE dataset present a high exogenous shock in the testing period. MLR, even in the presence of known information about the external stimuli, largely misses the predictions (as shown in Fig. 9 (b)). The Hawkes intensity model achieves levels of forecasting performance on the high exogenous dataset similar to the entire ACTIVE dataset. Fig. 9 (c) shows the distribution of absolute forecasting error for Hawkes (#shares) and MLR (#shares). Compared to Figure 8 (c), the Hawkes intensity model achieves smaller errors, with a median value of 3.25%, while MLR presents an increased concentration of high errors and a median value of median value 6.5%.

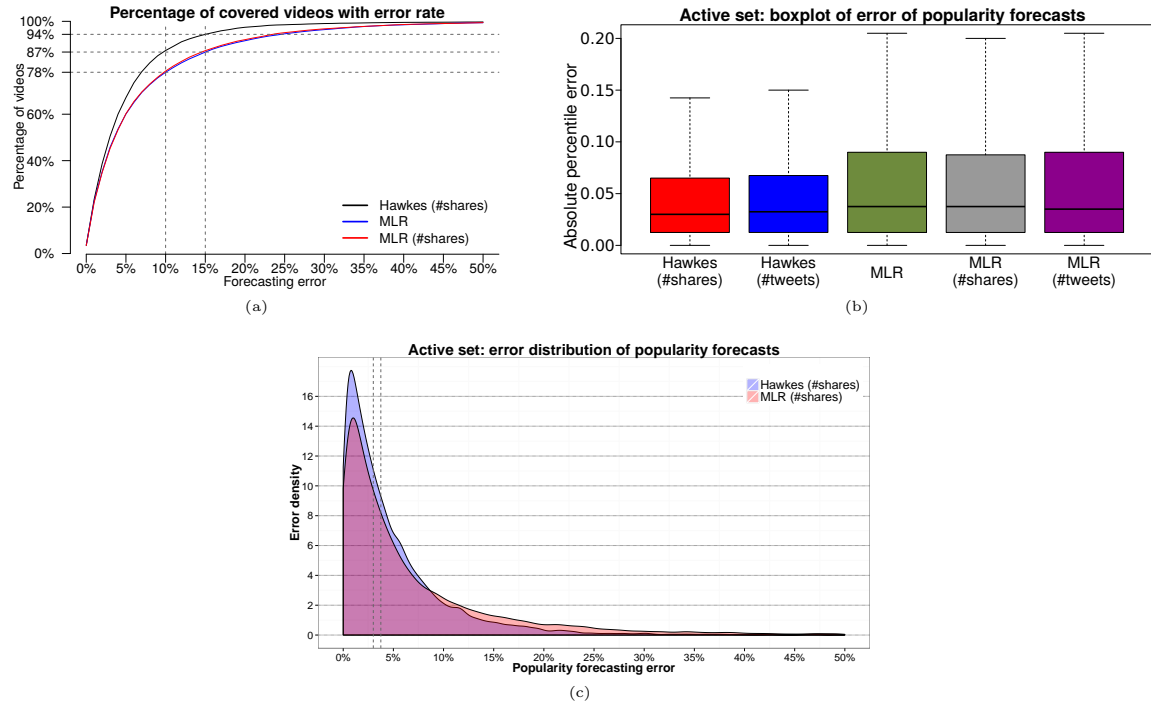


Figure 8: Performance comparison graphics, additional to Main Text: number of covered videos, when accepting a given error percentage (left) and barplots of absolute forecasting error (right). (bottom) Absolute forecasting error distribution for Hawkes (#shares) (blue curve) and MLR (#shares) (red curve). Median values are represented for each approach with gray vertical lines: 3% for Hawkes and 3.75% for MLR.

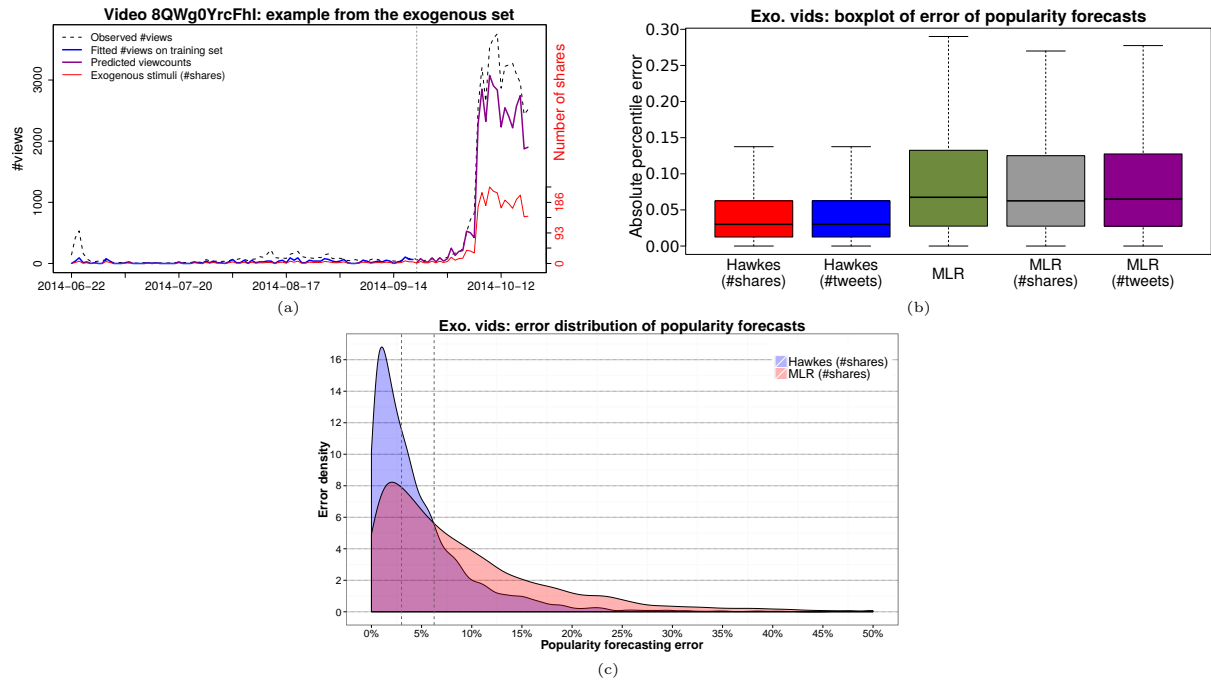


Figure 9: Forecasting performance for the Hawkes intensity model and MLR on videos presenting a high exogenous shock. (left) Depiction of a video having a high exogenous shock during the testing period. It is a relatively obscure video about Brazilian politics, which suddenly received a considerable amount of attention in October/November 2015 (more than 3 months after its upload), only to slide back into obscurity after December 2015. (right) Barplot aggregation of performances of Hawkes intensity and MLR (with different sources of external stimuli), in terms of absolute forecasting error. (bottom) Absolute forecasting error distribution for the exogenous set for Hawkes (**#shares**) (blue curve) and MLR (**#shares**) (red curve). Median values are shown with gray vertical dotted lines (3.25% for Hawkes and 6.5% for MLR).

1. Clauset, A., Shalizi, C.R., Newman, M.E.J.: Power-Law Distributions in Empirical Data. *SIAM Review* 51(4), 661–703 (Nov 2009).
2. Cohen, J.: *Statistical Power Analysis for the Behavioral Sciences*. Lawrence Erlbaum Associates, Hillsdale, NJ, 2nd edn. (1988).
3. Crane, R., Sornette, D.: Robust dynamic classes revealed by measuring the response function of a social system. *Proceedings of the National Academy of Sciences* 105(41), 15649–15653 (2008).
4. Granger, C.W.: Investigating causal relations by econometric models and cross-spectral methods. *Econometrica: Journal of the Econometric Society* pp. 424–438 (1969).
5. Hawkes, A.G.: Spectra of some self-exciting and mutually exciting point processes. *Biometrika* 58(1), 83–90 (Apr 1971).
6. Helmstetter, A., Sornette, D.: Subcritical and supercritical regimes in epidemic models of earthquake aftershocks. *Journal of Geophysical Research: Solid Earth* 107(B10), ESE 10–1–ESE 10–21 (2002).
7. Johnson, S.G.: The NLOpt nonlinear-optimization package (2011).
8. Liptser, R.S., Shiryaev, A.N.: *Statistics of Random Processes*. Springer Berlin Heidelberg, Berlin, Heidelberg (2001).
9. Liu, D.C., Nocedal, J.: On the limited memory BFGS method for large scale optimization. *Mathematical Programming* 45(1-3), 503–528 (aug 1989).
10. Miritello, G., Lara, R., Cebrian, M., Moro, E.: Limited communication capacity unveils strategies for human interaction. *Nature Scientific Reports* 3 (Jun 2013).
11. Ogata, Y.: Seismicity Analysis through Point-process Modeling: A Review. *Pure and Applied Geophysics* 155(2-4), 471–507 (1999).
12. Pfaff, B.: Var, svar and svec models: Implementation within R package vars. *Journal of Statistical Software* 27(4) (2008).
13. Pinto, H., Almeida, J.M., Gonçalves, M.A.: Using early view patterns to predict the popularity of youtube videos. In: *Proceedings of the sixth ACM international conference on Web search and data mining - WSDM '13*. p. 365. ACM Press, New York, New York, USA (Feb 2013).
14. Sullivan, G.M., Feinn, R.: Using Effect Size-or Why the P Value Is Not Enough. *Journal of graduate medical education* 4(3), 279–82 (sep 2012).

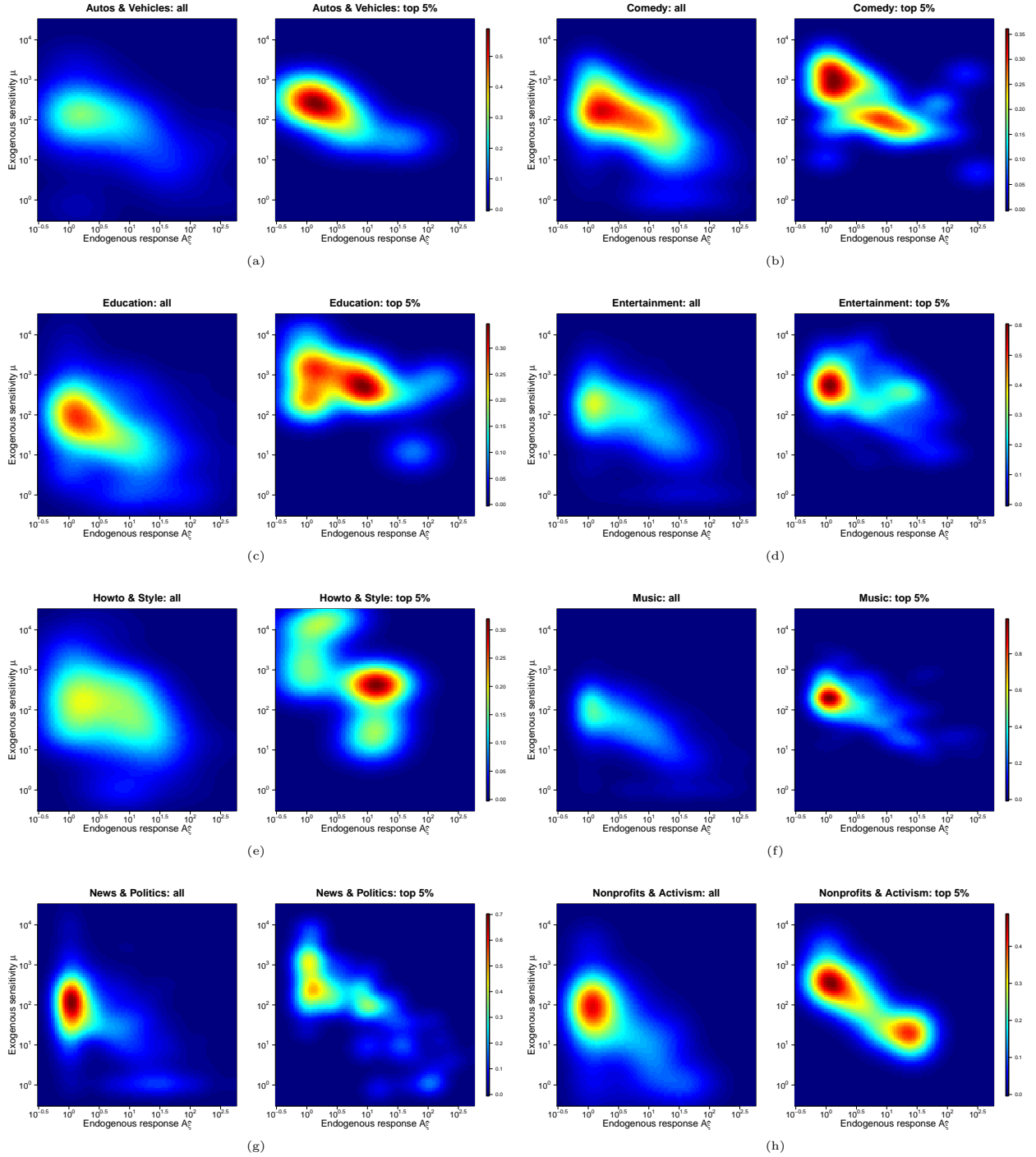


Figure 10: Pairs of 2-dimensional densities of videos on the endo-exo map, for each of the video categories in ACTIVE dataset (except for Gaming and Film & Animation, already presented in the Main Text Fig. 3). For each pair, the left heatmap represents the density distribution of all videos in the category, while the right heatmap shows the distribution of the most popular 5% videos in the category. 6 more categories are shown in Fig. 11.

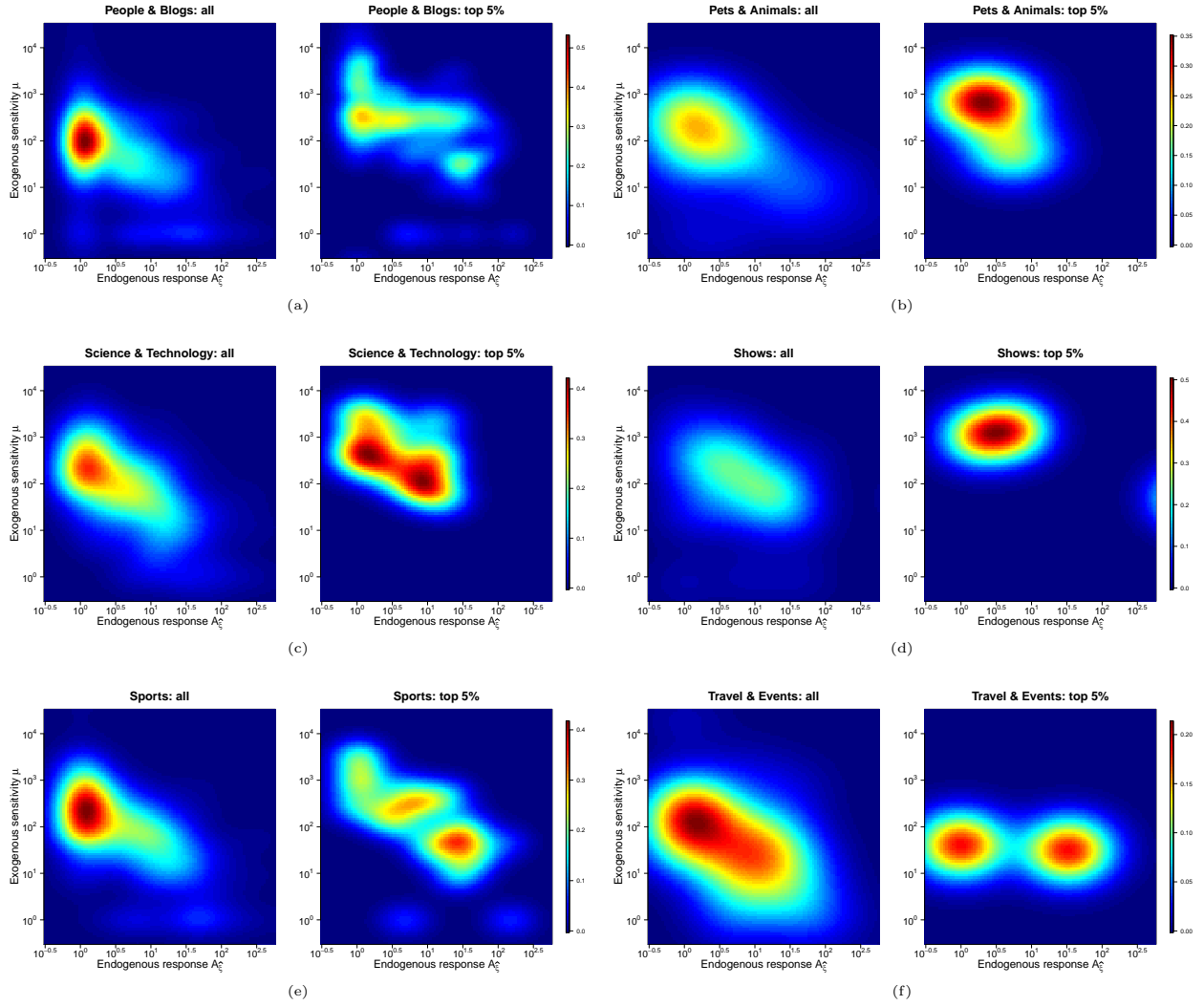


Figure 11: Fig. 10 cont'd: remaining categories.